Integrating GPR and ice-thickness models for improved bedrock detection: the case study of Rutor temperate glacier

Andrea Vergnano[1,2], Diego Franco[1], and Alberto Godio[1]

[1]Department of Environment, Land and Infrastructure Engineering (DIATI), Politecnico di Torino, Torino, Italy
[2]Department of Earth Sciences, Università degli studi di Torino, Torino, Italy

Correspondence: Andrea Vergnano (andrea.vergnano@polito.it, andrea.vergnano@unito.it)

Abstract.

Estimating the volume of glaciers has been researched with increasing interest because the cryosphere has rapidly evolved during the last decades of global warming. In temperate glaciers, the widespread englacial water content often challenges the analysis of Ground Penetrating Radar (GPR) data, the most used geophysical technique to investigate glacier ice thickness. In a past GPR survey, the Rutor glacier (European Alps) was supposed to store about 150 million m^3 of ice in 2008, but this estimate proved unrealistic after analyzing the geodetic mass balance data of the following decade. This study develops on the idea that ice-thickness models can help the GPR data analyst to better recognize the ice-bedrock interface in the radargrams. We selected three models, OGGM, GlabTop2 and GlaTE, which estimate bedrock topography starting from surface topography, following principles of ice flow theory, ice dynamics and mass conservation. Visualizing together GPR and model data in 2D and 3D helped the analyst to manually select the ice-bedrock interface, especially where the GPR data was scattered and interpretation uncertain. The GPR data were then used to constrain one of the models, GlaTE, in order to produce an ice-thickness map that is the result of both model estimate and GPR information: according to this methodology, the Rutor glacier stored about 450 million m^3 of ice in 2021, about three times the previous estimate. The analysis of more than one approach, and a simple sensitivity analysis on the GlaTE model, allowed to estimate the ice-thickness uncertainty linked to the use of models and GPR. The whole workflow was made openly available in the supplementary materials and may improve future GPR surveys of temperate glaciers, especially when facing scattered data due to englacial water content or other sparse reflectors such as debris. More accurate ice-thickness estimations will improve local studies and provide better calibration data for regional studies.

1 Introduction

Temperate valley glaciers are a characteristic feature of mountain chains in temperate zones, such as the European Alps, and have a pivotal role in the hydrological cycle (Milner et al., 2017). Studying the glacier processes and changes linked to the current climate crisis often requires a central task: a reliable estimate of their present-day ice-thickness distribution and geometry: bedrock topography, crevasses, cavities, debris, and englacial water (Haeberli et al., 2019). Such temperate glaciers are characterized by containing temperate (or "warm") ice at the melting point. Indeed, colder ice zones often exist in temperate glaciers, but they are limited to specific areas or seasons, e.g. where the snow melts late in the warm season, or in the areas

where the ice is thin and provides little isolation to the geothermal heat during the cold season (Suter et al., 2001; Reinardy et al., 2019). Temperate glaciers at the pressure melting point are primed for rapid meltwater production upon small energy or heat inputs.

A high englacial water content in glaciers can challenge the interpretation of bedrock returns from Ground Penetrating Radar (GPR), one of the most used techniques for surveying ice masses (Colucci et al., 2015; Forte et al., 2015; Urbini et al., 2019). Since englacial water has very different electrical permittivity compared to ice, it reflects and scatters the electromagnetic wave, hindering the signal from traveling until the bedrock and being detected on its way back (Reinardy et al., 2019). Smaller-scale heterogeneities, such as small fractures or sediment grains smaller than about a quarter wavelength, generate weak or undetectable responses, but their presence has an impact on the signals as they pass by. The heterogeneities extract energy as the electromagnetic field passes and scatter it in all directions (Jol, 2009). Langhammer et al. (2019b) studied the effects of antenna orientation on detection of the bedrock reflection. Challenges in detecting basal returns over temperate glaciers have been studied by Rutishauser et al. (2016), who analyzed a large set of GPR data acquired on Swiss glaciers and found that depending on the specific glacier, the bedrock interface could only be successfully detected in 12-69% of the data due to this scattering issue. GPR signal scattering rarely occurs in arctic cold glaciers, but when it is detected in some areas, it may be evidence that temperate conditions and englacial water are the cause (Karušs et al., 2022). Another common source of noise in GPR sections is the presence of debris at the surface of glaciers, as noted by Colombero et al. (2019), or at depth, due to phenomena such as adfreezing and entrainment of sediments into the basal ice layer (Weertman, 1961). Air bubbles trapped in ice cause scattering of GPR signal, which helps differentiate between various types of ice, such as firn and superimposed ice (Langley et al., 2009).

To study and address this scattering problem, we focus on the Rutor Glacier, the third-largest glacier in the Aosta Valley, Southern Europe Alps. Located in the southwestern European Alps, the Rutor massif hosts the third-largest glacier in the Aosta Valley. The massif develops on multiple terraces, on which the Rutor Glacier has advanced or retreated during the last centuries according to the climate variations, shaping the basin morphology, as reviewed by Vergnano et al. (2023). Nowadays, the Rutor Glacier (RGI ID: RGI60-11.03039) covers an area of 7.5 km^2 and it is situated in the municipality of La Thuile. It has retreated, since the beginning of 1900, to an upper terrace, forming new proglacial lakes near each of its three tongues (western, central, and eastern). Its tongues are situated on the northern side of the glacier at about 2550 m a.s.l. (the eastern tongue) and 2650 m (the central and the western tongue). Its highest elevation is about 3440 m, near the southern margin.

In recent decades, the glacier has experienced an accelerated retreat, linked to climate warming (Corte et al., 2024; Gizzi et al., 2022). By differencing 2021 and 2008 DEMs, pixel by pixel, we observed the changes in the glacier surface topography from 2008 to 2021. This simple analysis evidenced a loss of more than 20 vertical meters of ice in about 1/4 of the current glacier area (especially in the tongue area) for a total ice volume loss of about 100 million m^3. The 2008 DEM was retrieved from the regional cartography (Val d'Aosta Region, 2008); the 2021 DEM is available in an open repository described by Corte et al. (2024). Previous GPR surveys (1996-2006) reported an average thickness of the glacier of 17.5 m (a volume of 150 million m^3 over an area of 8.5 km^2) (Villa et al., 2008, 2007). However, this estimate does not agree with the ice lost from 2008 to 2021, because if both data were true, it would mean that the Rutor Glacier had shrunk to only 1/3 of its volume, from

2008 to 2021. Instead, while its shrinking is evident, it actually interested a relatively minor area at the lowest altitudes. We hypothesize that the ice volume estimate of 150 million m^3 could be far from the actual value, and that this issue may be due to problems in interpreting scattered GPR data. The analysis performed on the same glacier by Viani et al. (2020) expresses similar considerations about the challenge of interpreting the correct bedrock geometry. Moreover, many examples of other alpine glaciers with a similar area consistently show greater ice thickness (Grab et al., 2021).

In this study, the Rutor Glacier is investigated with two new GPR datasets, acquired in May 2012 with a helicopter-based survey (Morra di Cella, 2024) and in May 2022 with a ground-based survey. These new datasets reveal high scattering of the radar signal over most parts of the glacier, demonstrating the difficulty in detecting the ice-bedrock interface. The scattering zone is often located at around 20 meters of depth, and may easily be misinterpreted as the ice-bedrock interface, possibly explaining the previous doubtful estimates of ice thickness (Villa et al., 2008).

To address this problem encountered on the Rutor Glacier, but common to other temperate glaciers, this study explores the idea that ice-thickness models may aid in the interpretation of scattered GPR sections, especially to fill the gaps in the most scattered survey sections. Those algorithms require, as input, the glacier surface topography, which can be retrieved for example by satellite imagery. Some models have obtained much acknowledgment in recent years, see for example the ITMIX project (Farinotti et al., 2017) in which many glacier models are compared on the same set of glaciers. One of the conclusions of that research is that considering an average output from different models provides a more reliable ice-thickness estimate than finely tuning just one model.

The ice-thickness modeling algorithms employed in this work are three different models, the open source GlabTop2 (Frey et al., 2014), OGGM (Maussion et al., 2019) and GlaTE (Langhammer et al., 2019a). The ice thickness is predicted using the three models. During the manual selection of the ice-bedrock interface in the GPR data, the results from the three models are superimposed on the radargram to help identify the most likely ice-bedrock interface, often submerged by noise due to the englacial water content. Finally, a second run of the GlaTE model constraints the estimate of the ice thickness using the ice-bedrock interface selected manually on the GPR data, providing a final model of the bedrock topography.

2 Methods

We present here an overview of the workflow, enumerating the main steps of the proposed methodology. Then, the next paragraphs analyze the methodology in more detail. For reasons of space, we did not detailed here all the technical steps needed to reproduce the workflow. The interested reader is suggested to download the supplementary material, organized following the same logic used here, which contain "readme.txt" files providing technical help.

1. Run three models (GlabTop2, GlaTE, OGGM), which, based on the surface topography, estimate the ice thickness. We calculated the ice-thickness average and standard deviation of the three models, to have an overview of the ice-thickness uncertainty.

2. Collect and analyze new GPR datasets from two acquisitions, a helicopter-based survey made in 2012 and a ground-based survey made in 2022. The GPR data is often scattered and difficult to interpret.

3. Extract the ice thickness estimated by the models in the same locations of the GPR paths, thanks to the v.sample tool of QGIS, GRASS plugin (QGIS Development Team, 2021), using a bilinear interpolation method.

4. Visualize the GPR data and the model estimations together, in 2D with RGPR, (Huber and Hans, 2018) and 3D with Paraview (Ayachit, 2015).

5. Manually select ("pick") the bedrock reflector in the GPR data with the help of the estimations from the three models, to reduce the chance of misinterpreted bedrock reflections. For analysis and discussion purposes, we divided the pickings into "sure" pickings, "guided by model" pickings, and "wrong" pickings.

6. Run the GlaTE model for a second time, constraining the estimations with the GPR data.

7. Run the GlaTE model multiple times, varying the input glaciological parameters, to perform a simple sensitivity analysis on both the unconstrained and the constrained-by-GPR version of the model.

8. Comparing the results with literature products.

2.1 Ice thickness models

The GlabTop2, GlaTE and OGGM models used in this study require as input a digital elevation model (DEM) of the glacier surface, and their algorithms are based on theoretical considerations of ice flow theory, ice dynamics and mass conservation. In this study, they were employed for two objectives. First, to provide a first estimate of the ice thickness distribution of the Rutor Glacier, in order to help identify the ice-bedrock interface in the GPR sections. Second, the GlaTE model (introduced later in this paragraph) was employed to provide a final estimation of the Rutor Glacier ice thickness, based on both model estimations and GPR data constraints.

The thickness inversion models required additional input parameters (e.g. ice density, Glen's exponent...). These were checked for consistency with the Rutor Glacier study area, but unless stated otherwise, default values from similar alpine glacier studies by the model developers were used. This is a simple choice that could induce some errors: in fact, these parameters are not really transferable between glaciers (Zekollari et al., 2022). For this reason, we performed a sensitivity analysis on the final model (see the specific paragraph).

The DEM and the glacier margin, manually drawn based on a high-resolution orthophoto, come from a topographical survey carried out in 2021 (Macelloni et al., 2022; Corte et al., 2024). With the warp/reproject tool of QGIS software, using a bilinear-based triangulation method, the DEMs were undersampled to 20-m resolution, for computation time optimization and because using a too-fine resolution showed to produce misleading structures in the resulting bedrock topography.

The features of the three models are described below.

2.1.1 GlabTop2

The GlabTop2 (Glacier bed Topography 2) model assesses the distribution of ice thickness in a glacier starting from a DEM file and a mask file containing the margin of the glacier (Frey et al., 2014). It employs an algorithm first developed by (Linsbauer et al., 2012), but slightly modified to avoid the laborious process of manually drawing branch lines:

$$h_f = \frac{\tau}{f \cdot \rho \cdot g \cdot sin(\alpha)} \tag{1}$$

where h_f is the mean ice thickness along the central glacier flow line, f is a shape factor, fixed at 0.8 (according to Haeberli and Hoelzle (1995); Frey et al. (2014)), τ the shear stress at the glacier base, calculated with an empirical formula based on the elevation range of the glacier ΔH (equation 2), and expressed in kPa, ρ the ice density (900 $\mathrm{kg/m^3}$) (Langhammer et al., 2019a), g is the gravity acceleration, and α is the surface topography slope.

$$\tau = 0.5 + 159.81\Delta H - 43.5\Delta H^2 \tag{2}$$

The first processing step employed by the algorithm is an initial approximation of ice thickness in some random cells of the domain, based on the surface slope of a sufficiently large buffer zone around the cell. Then, the ice thickness of the remaining cells is estimated with a simple inverse distance weighting algorithm. The two steps are repeated for n times and the results are averaged.

The code is open source, runs in Python, and is available in an open repository (Terink, 2018). Further details are provided in the appendix of Frey et al. (2014). In the supplementary materials, the GlabTop2 model code adapted for this case study is available to ensure full reproducibility. Among the various folders and files, the config.cfg file contains a little section about the input parameters used in this study.

2.1.2 GlaTE

GlaTE (Glacier Thickness Estimation) is also based on equation 1, but with a different estimation of the shear stress τ and a different implementation algorithm, according to the work of Clarke et al. (2013). In this work, it was employed in two separate steps: first, to provide an initial estimate of the glacier thickness, together with the other two models, and secondly, to calculate a final estimate of the ice thickness with known ice thickness points (from GPR data) constraining the model. In fact, the strength of GlaTE is the integration between the estimation model (based on surface DEM and glacier margin like GlabTop2) and ground-proof data derived from GPR profiles. GlaTE performs an inversion procedure, constraining the ice thickness results such that they match, with a certain degree of uncertainty, a series of ground-proof data, such that they follow some smoothness requirements, respect the glacier perimeter, and the values at the border of the glacier are consistent with the

terrain slope outside the glacier. The system of equations to be inverted can be summarized into the matrix in equation 3 :

$$\begin{bmatrix} \lambda_1 G \\ \lambda_2 L \\ \lambda_2 B_{gb} \\ \lambda_3 B_0 \\ \lambda_4 S \end{bmatrix} h_{est} = \begin{bmatrix} \lambda_1 h_{GPR} \\ \lambda_2 \nabla h_{Clarke} \\ \lambda_2 \nabla h_{boundary} \\ \lambda_3 \\ \lambda_4 \end{bmatrix} \tag{3}$$

where h_{GPR} is the ground proof GPR-derived ice thickness, h_{Clarke} is the ice thickness modeled according to Clarke's algorithm, ∇h_{bound} is the gradient of terrain slope at the boundary of the glacier. The operator G ensures the constraint with GPR data, L with the ice thickness modeled according to Clarke's algorithm, B_{gb} with the slope outside the glacier, B_0 with the 0 thickness at the boundary, while S is a smoothing constraint. The λ factors are weighting factors and are varied in an iterative manner, in order to give maximum weight to the Clarke model and the smoothness constraint while fitting the GPR data (Grab et al., 2021). The ice density was estimated at 900 $\mathrm{kg/m^3}$. The creep factor (or ice softness) A was estimated to be about $2.4 \cdot 10^{-24}\ \mathrm{s^{-1}Pa^{-3}}$, neglecting its temperature dependence as if the glacier was at 0°C (Cuffey and Paterson, 2010), since the Rutor Glacier shows temperate conditions (even if this could not be true for the entire glacier) (Cook et al., 2020). The exponent of Glen's flow law was fixed at 3, as considered the best approximation in the absence of data about the ice fabric (Glen and Paren, 1975). Eventual debris presence, which can be added to the model, was not taken into consideration, because from the orthophotos, and by visual investigation, there is no evident thick debris cover in the ablation area of Rutor Glacier. For further details, see Langhammer et al. (2019a); Grab et al. (2021); Schwanghart and Scherler (2014).

The model is open source, it runs in MATLAB environment and is available in an open repository (Maurer, 2022). In the supplementary materials, the GlaTE model code adapted for this case study is available to ensure full reproducibility. Among the various folders and files, the parameters.txt file in the Matlab folder contains the input parameters used in this study.

2.1.3 OGGM

The OGGM (Open Global Glacier Model) is an open-source collection of algorithms written in Python that provides different insights about glaciers, for example, thickness, meltwater runoff, and future predictions based on climate variations. Its main aim is regional-scale modeling, but the code is modular and can be adapted to work on a single glacier. In this work, the OGGM version 1.6.2 was used, and only the OGGM ice thickness inversion algorithm was employed, which is based on ice flow dynamics and mass conservation (Farinotti et al., 2009; Maussion et al., 2019). The ice flux is computed as equation 4:

$$q = uS = \left(f_d h \tau^n + f_s \frac{\tau^n}{h} \right) S \tag{4}$$

where h is the ice thickness, q is the ice volume flux, u is the ice flow velocity, S is the section, which in case of a simplified parabolic section is $= 2/3 \cdot h \cdot width$, n is the exponent according to Glen's law (=3), τ is the shear stress, f_d is proportional to the ice softness A ($f_d = 2A/n + 2$), f_s is a sliding factor, neglected for simplicity in this run of the model. The flux q in a section is also equal to the mass balance (mass input - output due to precipitation and melting) integrated over the area of the

glacier situated above the section considered. This model, in its latest version, works even without the equilibrium assumption, calibrating the mass balance parameters thanks to a geodetic mass balance calibration (Hugonnet et al., 2021). The climate data are taken from the W5E5 dataset (Lange, 2019). During the inversion process, one parameter, the ice softness A, is calibrated against a regional consensus ice volume (Farinotti et al., 2017) and it is allowed to vary, in general about one order of magnitude, from the standard value of $2.4 \cdot 10^{-24}\ \mathrm{s}^{-1}\mathrm{Pa}^{-3}$.

Further details and the implementation in the OGGM framework are described in Maussion et al. (2019) and the software is freely available in an open repository (Maussion, 2024). In the supplementary materials, the OGGM model code adapted for this case study is available to ensure full reproducibility. Among the various folders and files, the .ipnyb Python Jupiter notebook contains a little section about the input and calibrated parameters used in this study.

2.2 Ground-penetrating radar (GPR)

Low-frequency antennas were employed to survey the thick ice layers of the Rutor Glacier. In the 2012 helicopter-based dataset, a GSSI single-frequency antenna with a central frequency of 70 MHz was employed. In the 2022 ground-based survey, a 40 MHz antenna, RIS ONE model with single-frequency antenna configuration, manufactured by IDS, was carried on ski by an operator. The location of the GPR profiles is shown in Figure 1.

The raw data were processed using the commercial ReflexW software (Sandmeier, 2012). The GPR data were processed by the following method:

1. Application of a background removal filter (x-direction average-trace removal over the entire profiles), to eliminate instrument noise constant in the x-direction.
2. Application of a bandpass butterworth filter, from 0 to 150 MHz, to eliminate high frequency noise.
3. Application of a make equidistant traces filter, to plot 1 trace per meter, especially important for the 2012 survey, since the helicopter was not flying constantly at the same speed.
4. Application of a gain filter called Energy decay: a gain curve in y-(time-) direction applied on the complete profile based on a mean amplitude decay curve, which is automatically determined (Sandmeier, 2012), to compensate the time-direction attenuation and geometric spreading of the signal.
5. Conversion of the y-axis from time to depth, assuming a constant velocity of the electromagnetic signal in the ice of 0.167 m/ns (Bohleber et al., 2017). For the helicopter-based survey, we also removed the part of the signal travelling in the air. We did not notice any interference from nearby slopes or features, as in other studies (Church et al., 2018): the helicopter was flying at a low altitude above ground and the most of the Rutor Glacier is not surrounded by steep slopes.
6. Manual selection of the ice-bedrock interface with the guidance of model estimations.

The data were not migrated. Some attempts with simplified velocity models were tried, without any significant enhancement.

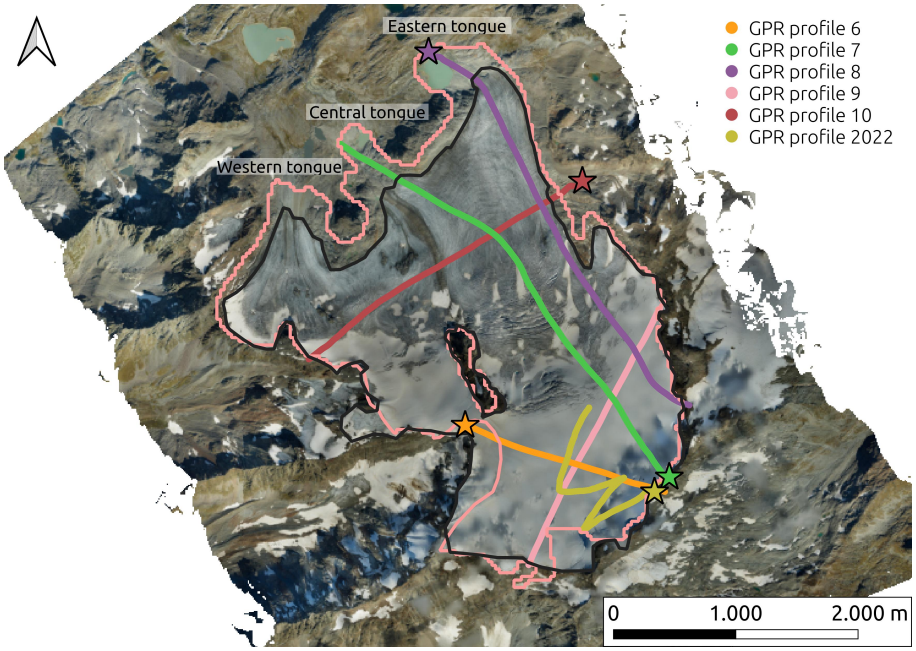

Figure 1. The GPR profiles of the Rutor Glacier survey. Star markers indicate the start of the profiles. Numbering from 6 to 10 is based on the numbering of the original helicopter-based dataset (Morra di Cella, 2024). The black glacier margin is that of 2021 used in this study (Macelloni et al., 2022). The pink glacier margin is the 2003 RGI outline (RGI Consortium, 2017).

2.3 2D and 3D visualization of GPR and models together - selection of the bedrock interface

After having run the three unconstrained models and had an overview of the ice thickness, we needed tools to visualize them together with the processed GPR data, making it possible to perform the selection of the ice-bedrock interface with the model guidance.

The first visualization tool that we employed is RGPR, open source software to analyze and process GPR data (Huber and Hans, 2018). Since it runs in the R environment, it was straightforward to slightly adapt the code to plot the ice thickness estimated by the models together with the GPR profiles. The visual overlap of GPR and models helped in picking the ice-bedrock interface.

A second visualization tool was experimented: a 3D map with surface topography, bedrock topography based on the three models, and GPR profiles, was built and visualized in Paraview (Ayachit, 2015). The aim of this tool is the same as the profile visualization made in RGPR. However, notwithstanding the drawback of being a little more complex to setup, it has a pair of advantages: first, the 3D visualization allows one to directly see where the GPR profiles intersect, helping recognize the ice-bedrock interface as it develops along different profiles; second, visualizing the whole glacier in a 3D environment is a better support to integrate the users local knowledge of the glacier, allowing them to better recognize the glacier shape and features and their correlation with ice thickness.

Some topographical adjustments were necessary to assist in analyzing GPR observations that span different time periods (2012 and 2022). Moreover, the DEM used as models input was acquired in another year, in 2021. In other words, the models represent the 2021 situation, and the GPR data corresponds to 2012 and 2022.

To compare the three ice-thickness models generated by the three algorithms with the GPR sections of the 2012 survey, every model had to be "converted" to 2012, that is, the ice lost from 2012 to 2021, had to be accounted for in the comparison. In fact, the ice lost in that time frame, especially in the lowest parts of the glacier, was not negligible, as shown in Figure 2. Since a good 2008 DEM of the glacier surface was available from the regional cartography (Val d'Aosta Region, 2008), the ice loss from 2012 to 2021 was estimated by a simple linear interpolation between the 2008 glacier surface elevation and the 2021 glacier surface elevation, supposing that the glacier melting in those years was constant on average. The calculated ice lost from 2012 to 2021 was added to the model thicknesses, to allow comparing them to the 2012 GPR sections. For comparing the 2022 GPR profile to the models, no correction was performed, since the ice lost from 2021 to 2022 is negligible for the kind of comparison performed, and the 2022 profile is situated in the highest portion of the glacier, where melting is minimal.

To perform these topographical adjustments and analysis we made sure that all data were reprojected into the same Coordinate Reference System (WGS84, UTM 32 N), using the warp/reproject tool of QGIS software.

Thanks to these visualization tools, the comparison between models and GPR could be done. The ice-bedrock interface was then manually selected ("picked") in ReflexW, assigning different codes (and colors) to "sure" pickings, "guided by model" pickings, and "wrong" pickings. The "wrong" pickings were selected in those portions of the GPR profiles where it could seem reasonable to "see" an ice-bedrock interface, but considering the whole picture of the glacier, by observing the glacier shape estimated by the models, and thanks to local knowledge, it is probably a false positive. Those "wrong" pickings have the only goal of showing the difficulties in interpreting scattered GPR data, and they were not used in the following analysis of the GlaTE model constrained by GPR data.

2.4 GlaTE model constrained by GPR and sensitivity analysis

After the manual selection of the reflectors in the GPR data, the final GlaTE model, constrained by GPR data, was run. To achieve this, the ice-bedrock interface manually selected on GPR data, based on the 2012 survey, was corrected to 2021, by subtracting the ice lost from 2012 to 2021 from the thickness. The GPR-based ice thickness was given an estimated error of 30% as GlaTE input parameter, to take into account the uncertain nature of the pickings due to the scattered data.

A simple sensitivity analysis was performed on the glaciological parameters A (creep factor [$\mathrm{s}^{-1}\mathrm{Pa}^{-3}$]) and gsi (fraction of creep relative to basal sliding [-]). The creep factor A varied from $1.2 \cdot 10^{-24}$ to $4.8 \cdot 10^{-24}$, $2.4 \cdot 10^{-24}$ being the standard value as suggested by Cuffey and Paterson (2010), while gsi varied from 0.25 to 0.75, 0.5 being the default value suggested by the model developers. In QGIS, we calculated the average and standard deviation of the various ice thickness models estimated with the different parameters, for both constrained and unconstrained GlaTE models.

3 Results

Figure 2 presents a map of the ice-thickness changes of the Rutor glacier from 2008 to 2021. As mentioned in the Introduction section, this analysis was also one of the main motivations of this study. Integrating the elevation variations over the glacier area, a total ice loss of 100 million m^3 was estimated. This estimate did not agree well with the previous total ice volume estimate of 150 million m^3 by Villa et al. (2008), based on a GPR survey, because it would have meant that only 50 million m^3 still remained in the glacier, which was improbable, given its size. This analysis prompted us to collect and analyze new GPR data to understand which were the sources of uncertainties in the GPR data that gave this results.

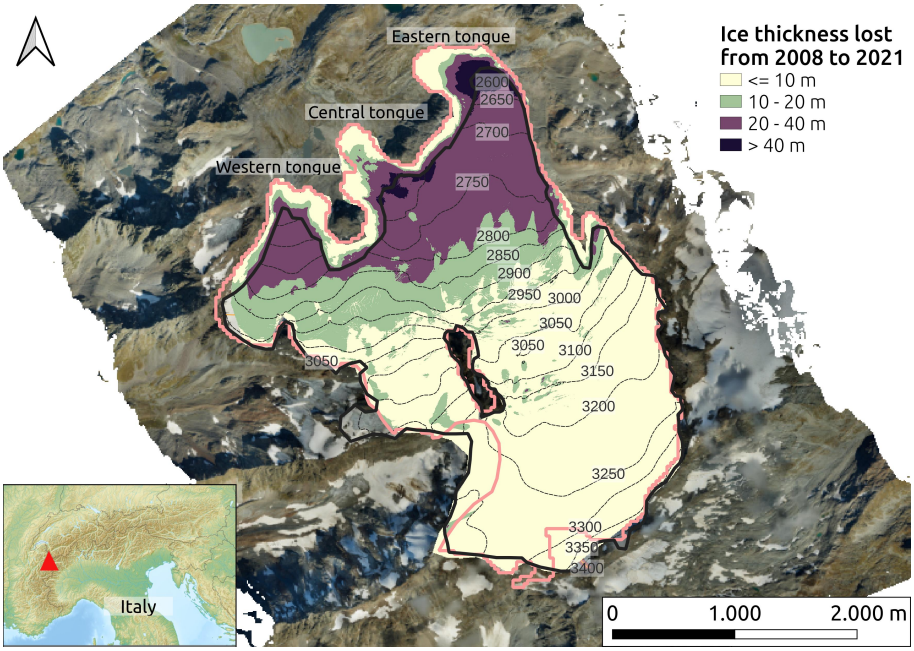

Figure 2. The Rutor Glacier (RGI ID: RGI60-11.03039) divided in four categories, according to changes in ice thickness (m) from 2008 to 2021 ("tokyo" color scale, according to Crameri (2021)). The black glacier margin is that of 2021 used in this study (Macelloni et al., 2022). The pink glacier margin is the 2003 RGI outline (RGI Consortium, 2017), and this choice is visible in the yellow areas near the three tongues of the glacier, which did not change in altitude from 2008 to 2021 because they were already free of ice in 2008.

The processed GPR sections on the temperate Rutor Glacier showed difficulties in interpreting GPR data, because they were affected by scattering and random noise. We acknlowledge that, probably, the analysis of previous GPR data could have been affected by this problem and could have been misinterpreted. Figure 3 shows an example section of the heli-based 2012 dataset. An omnipresent clutter zone is situated at 10-50 m of depth, and could be easily misinterpreted for the true bedrock, fortunately visible in the right part of the profile.

Looking at the central part of Figure 3, one could be tempted to interpret the area without reflections, pictured in white, as ice, and the first strong backscatter zone, omnipresent in the profile at 10-50 m of depth, as the bedrock. However, on the right

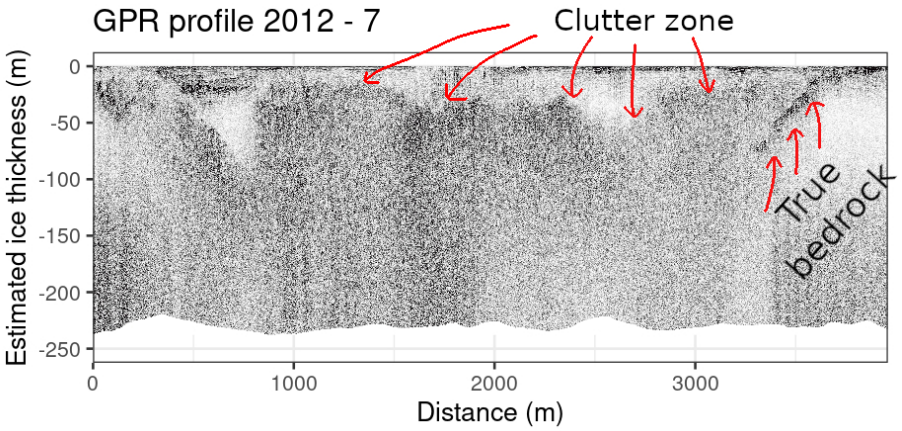

Figure 3. The GPR section number 7 of the heli-based 2012 dataset. The thickness scale was built assuming a constant velocity of the electromagnetic signal in ice of 0.167 m/ns. The white area is compact firn or ice without water. The ice-bedrock interface is well visible only on the right part of the image.

side of the plot, the ice-bedrock interface that submerges below the backscatter zone suggests that the former backscatter area is probably not a bed return, even if it looks like it. Elsewhere, possible ice-bedrock interfaces may be spotted and somewhat followed in the GPR section, but the interpretation is far from straightforward.

Therefore, a help was needed to get a general idea of where the bedrock could be situated. This help came from the three ice-thickness models (GlabTop2, GlaTE, and OGGM) shown in Figure 4, which estimated the bedrock position based on the surface topography, ice flow theory, ice dynamics and mass conservation.

The three raster maps in Figure 4, although produced with different models, showed a very similar reconstruction of the glacier geometry. The total ice mass estimated by the models was consistently higher than the 150 million m^3 of the previous estimate, and it was about: OGGM = 630, GlaTE = 510, GlabTop2 = 580 million m^3.

To visualize the model estimation together with the GPR data, their thickness value was bilinearly interpolated at the points corresponding to the GPR survey paths. Figure 5 shows an example ice-thickness profile extracted from the previous models, matching the location of a GPR section, used as a base to manually select more easily the reflections of the ice-bedrock interface. All the other GPR sections with the model estimations are shown in detail in the Appendix. The manual selection of the bedrock interface was indicated in the figures with different colours, to distinguish the "sure" pickings, the probably "wrong" ones, and those guided by the models. Moreover, a 3D environment was set up in Paraview software to better visualize the GPR profiles as they intersected between each other and the modeled bedrock. This visualization tool enhanced the visual interpretation of the GPR data, and an example is given in the Appendix, in Figure A7. Average and standard deviation plots, as well as a main flowline profile, are also included in Figure 4.

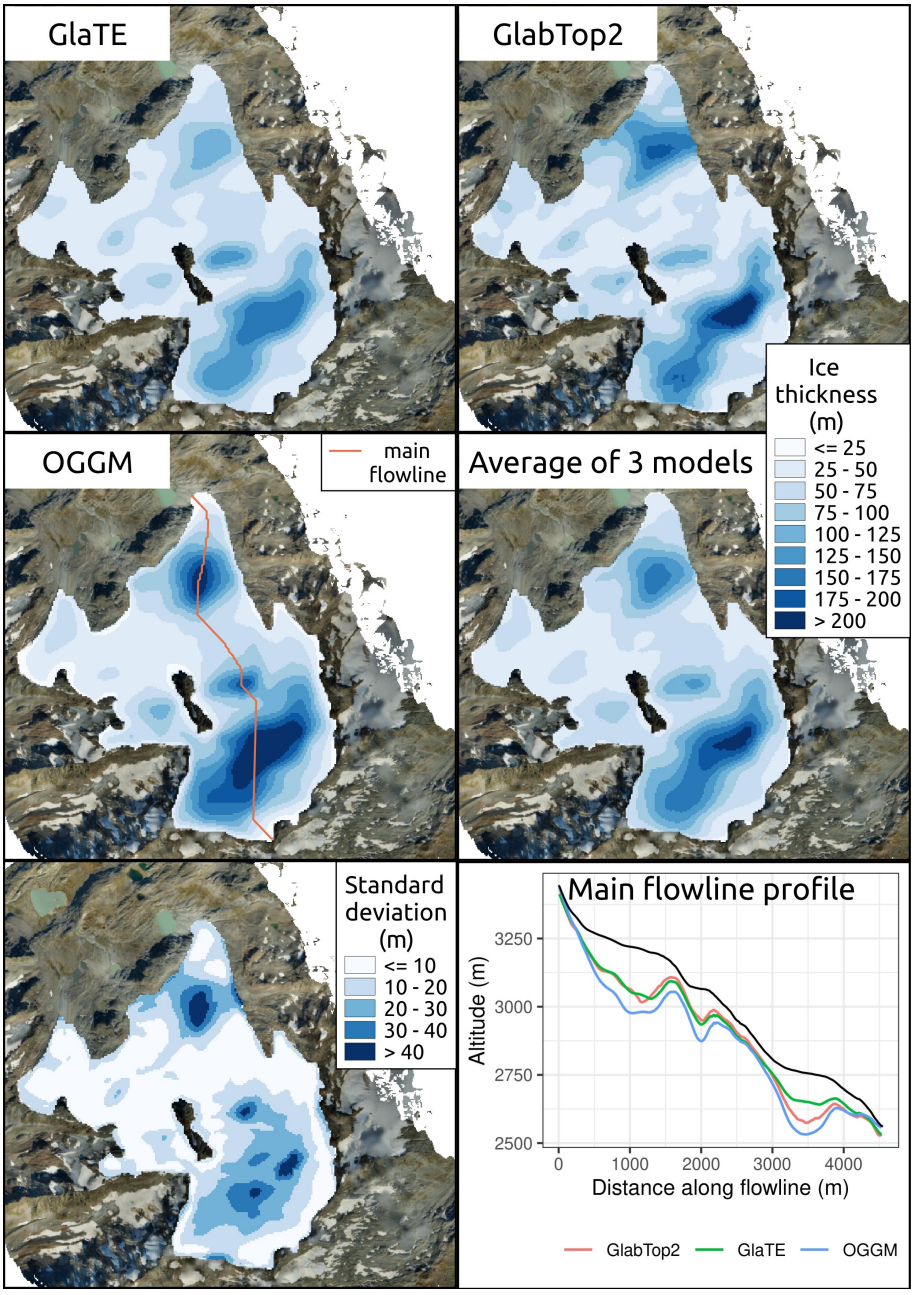

Figure 4. Ice thickness maps of the Rutor Glacier produced with GlaTE, GlabTop2, and OGGM models without any constrain by ground-proof data, but only with topographic surface data as input.

The bedrock interface selected in the GPR data was then imported into the GlaTE model to perform a constrained run. Figure 6 shows the results of the last GlaTE inversion, performed constraining the model with the manually selected ice-bedrock interface of all the GPR profiles. The total ice volume calculated in this way was about 450 million m^3

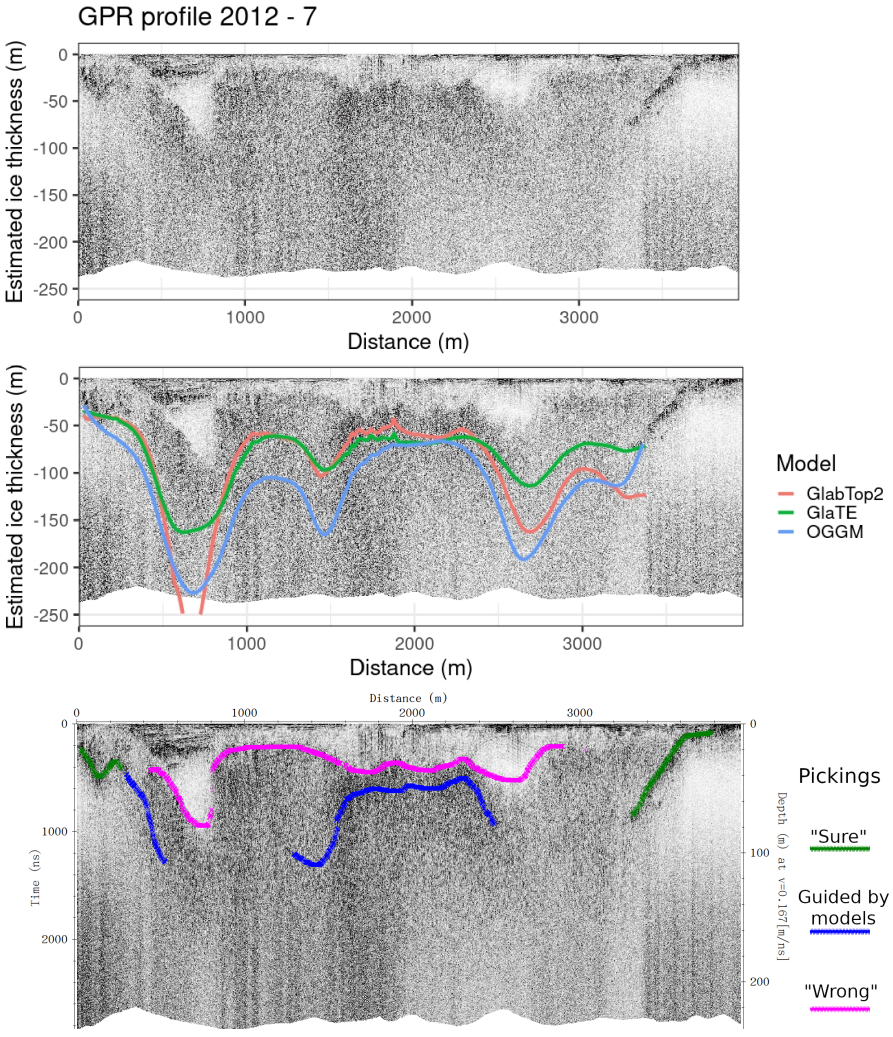

Figure 5. An example GPR section with the estimation from the three models overlayed: GlabTop2 in red, GlaTE in green, OGGM in blue. The manual selection of the ice-bedrock interface, which was possible by comparing the GPR profiles and the models, is displayed in different colours according to their .

Figure 7 shows the results of the sensitivity analysis on the final GlaTE model, in both its unconstrained and constrained version. Maps of average and standard deviation are shown, as well as a profile visualization. By varying the input glaciological parameters A and gsi, the unconstrained version of the model experienced a standard average variation of +- 75 millions m^3 of ice, whereas the variation of the constrained model was negligible.

In Table 1 we report the ice volume estimates of the different models employed in this study, as well as some literature products from Farinotti et al. (2019), Millan et al. (2022) and Villa et al. (2008).

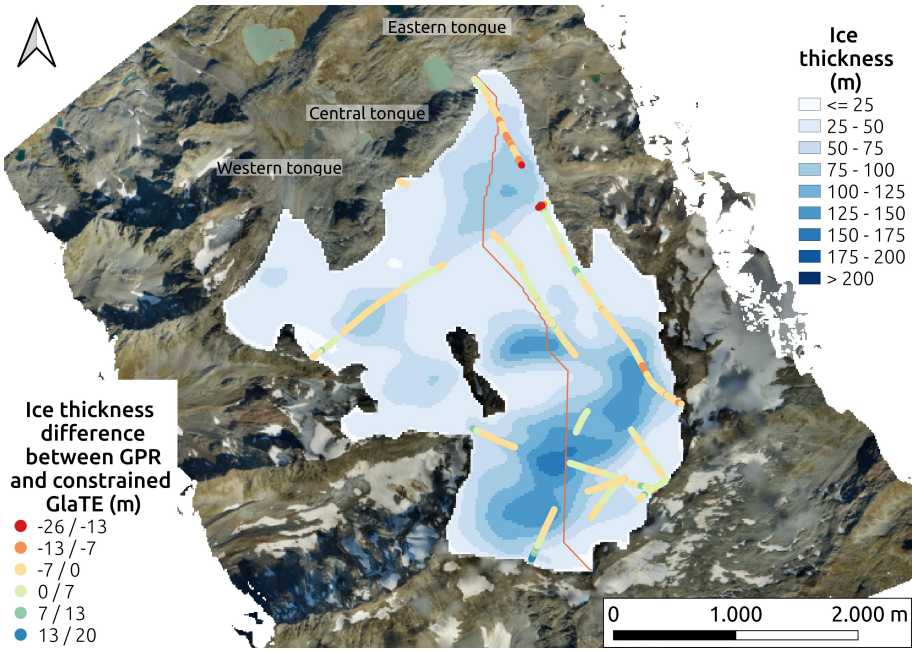

Figure 6. The final model of the Rutor Glacier ice thickness obtained by GlaTE model constrained with the GPR data. The pickings of GPR data are shown as differences between GPR ice thickness and GlaTE ice thickness. The final GlaTE model was fairly consistent with the GPR input data.

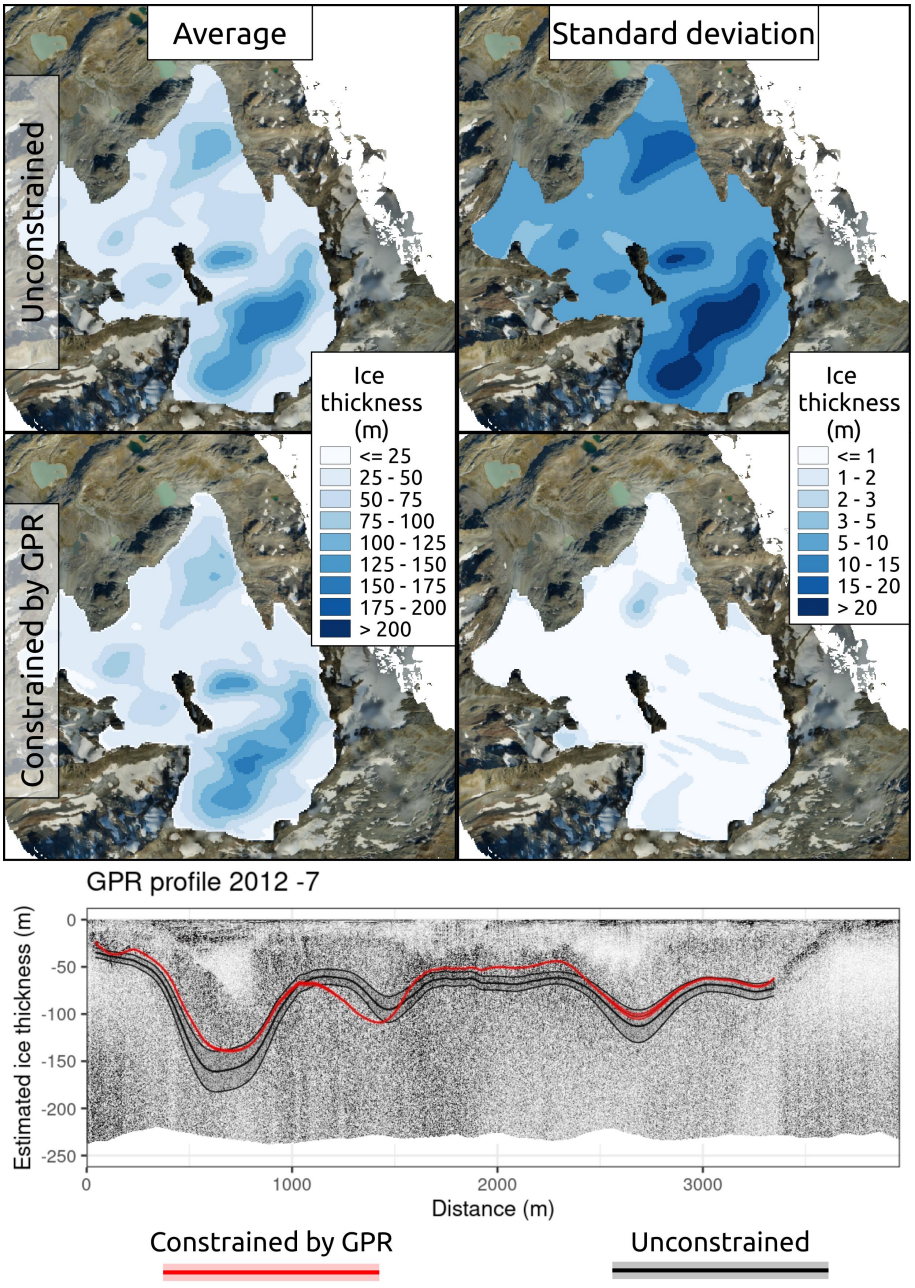

Figure 7. Sensitivity analysis plots on the unconstrained (top 2 plots) and constrained (middle 2 plots). Profile 7 view of the sensitivity analysis (bottom plot).

Table 1. Ice volume comparison between the different ice-thickness products of this study and literature.

Model	Ice volume (million m3)
OGGM	626
GlabTop2	577
GlaTE (unconstrained)	512
Average of 3 models	569
Standard deviation	100
GlaTE (constrained by GPR)	452
Consensus (Farinotti)	631
Millan	634
Villa et al. (2008)	150
Sensitivity analysis on GlaTE model	
GlaTe average (unconstrained)	507
GlaTe standard deviation (unconstrained)	75
GlaTe average (constrained)	451
GlaTe standard deviation (constrained)	4

4 Discussion

4.1 Comparison of the three ice-thickness models

The three different models, in their first run without GPR constraints, gave fairly similar estimates of ice volume (OGGM = 630; GlaTE = 510, GlabTop2 = 580 million m^3), with an average of 570 million m^3. Setting the resolution of the models at 20 m avoided the exaggeration of over-deepenings in the glacier bedrock that was a result of a too fine resolution. However, the distribution of standard deviation shows that the most uncertain areas are those with overdeepenings. The OGGM estimations were qualitatively similar to those of GlaTE and GlabTop2 (which both use the perfect plasticity method), except in some minor parts, notwithstanding their differences in the algorithms employed. The OGGM higher estimated volume is probably due to its mass balance calibration against the consensus estimate (Farinotti et al., 2019), which estimated a volume of about 630 millions m^3 (Table 1 and Figure A9). The consistency between different models, especially in terms of the general shape of the glacier, was already observed in a previous review (Farinotti et al., 2017), which stated that models based on surface topography can provide fairly accurate estimations of ice thickness. They can provide gross estimates of ice volume or future position of lakes in place of glacier overdeepenings (Viani et al., 2016), with a lower effort in terms of input data and computational time compared to a GPR survey. However, the performance of the models was poor near the margin of the glacier: here, the thickness was generally overestimated compared to the GPR data. We suppose that this fact could be due to the simplification of the glacier geometry and interpolation procedures used by the models, which work better in elongated-shape valley glaciers, but perform worse in wider and more complex glaciers such as the Rutor glacier.

4.2 Joint interpretation of GPR and ice-thickness models

GPR and ice-thickness models were interpreted together in all the GPR sections of the Rutor Glacier, which were both helicopter- and ground-based. The various GPR sections had a different degree of strength of the bedrock return. In some of them, the ice-bedrock interface could be followed relatively easily, such as for section 2012 - 8 (Figure A3). In that case, the three models (GlaTE, GlabTop2, OGGM) were generally consistent with the ice-bedrock interface depicted by the GPR reflections, demonstrating the overall good quality of the retrieved ice-thickness, already proven by Farinotti et al. (2017). In most other sections the bedrock was rapidly lost below about 50 m of depth. In general, the signal suffered from scattering, due to the many reflection events distributed throughout the glacier, except in some areas near the margin. This phenomenon made the interpretation of these sections challenging. In this sense, the ice-thickness models were fundamental to retrieving the bedrock topography where it could not be detected by the GPR and to avoid misinterpretations. Especially, in the parts of the profiles where all three models indicated the same ice thickness, we were more confident in picking that ice thickness as the correct one, provided that it was a reasonable interpretation of the GPR data, although scattered. No particular improvement was seen when using a ground-based 40 MHz GPR antenna compared to the heli-based 70 MHz antenna. Specific comments on the interpretation of each GPR section are available in the Appendix section, which we invite the readers to look at, because they are different examples of how problematic GPR profiles were interpreted thanks to this methodology, and which kind of mistakes were avoided.

This joint interpretation prevented the mistake of interpreting the first non-reflective layer (white in the GPR sections) as ice and the first reflective zone (scattered black) as bedrock. The deepening reflection on the right side of Figure 3 clearly shows that the ice-bedrock interface is not related to the scattered reflective zone observed at 20-40 m depth. Manually picking the ice-bedrock interface, guided by the estimates from the models, was particularly helpful, especially below 50 m, where the GPR signal was too attenuated. A possible source of uncertainty in detecting the correct ice-bedrock interface may also be due to off-nadir reflections, i.e. from valley side walls. However, we do not think this issue is critical in this glacier, which is large and has no steep side valley walls.

The ice thickness estimated with the second run of the GlaTE model constrained by GPR data is about 450 million m^3, which is not extremely far from the GlaTE estimate without GPR data (510 million m^3). Partially, the estimate of the GlaTE constrained model is lower because the models tended to overestimate the thickness near the glacier outline, an issue that was mitigated by the GPR data in the constrained model. The final estimate of 450 million m^3 is almost three times larger than the 150 million m^3 previously calculated (Villa et al., 2008). Two literature ice-thickness products were compared to this result, the consensus estimate by Farinotti et al. (2019) and a velocity-based model by Millan et al. (2022). Those models showed consistency between them in terms of volume estimate (about 630 million m^3, even if the bedrock shape was quite different (Figure A9). The higher volume estimation compared to the GlaTE model is probably due to the fact that this product still relies on the 2003 RGI outline (RGI Consortium, 2017), quite out of date due to the rapid shrinking of the glacier. A question arises, if those ice-thickness products be used instead of running the three models, for the same goal of helping to select the correct bedrock interface in the GPR radargrams. While it would surely be much simpler, one has to take into account that ice-thickness products built from regional scale studies not always benefit from updated glacier outlines (which are changing rapidly), and it is more difficult to extract insight about model uncertainty (e.g. by sensitivity analyses).

4.3 Advantages and limitations of the methodology

Without the help of ice-thickness models, a small part of the GPR profiles clearly identified the bedrock. This is not an ideal situation to draw a thickness map of the glacier, and it is argued that a similar interpretation problem could have arisen in the 2006 dataset analyzed by Villa et al. (2008), explaining the unexpectedly shallow thickness calculated there. This clutter phenomenon has been previously reviewed by Rutishauser et al. (2016), which observed that, depending on the glacier, only from 12 to 69 % of the bedrock could be identified. This review was performed on Swiss glaciers, which have climatic conditions similar to the Rutor Glacier. Moreover, better results were achieved only in alpine glaciers where cold conditions are more widespread. Therefore, this methodology could represent a tool to increase the "pickable", or "selectable" regions of scattered GPR sections. This methodology can help especially in the areas where generally GPR is more difficult to interpret: where the ice is thickest, where the bedrock slope is highest, and where there is englacial water (Rutishauser et al., 2016). In the dataset analyzed here, the higher ice thickness is recognized to be a cause of lower clearness of GPR sections, and englacial water content is highly probable, given the scattered GPR sections and the relatively warm climate in which the Rutor Glacier is situated. In the GPR profiles, we highlighted in purple the possibly “wrong” pickings, which represent the clutter zone easily misinterpreted as bedrock, without the model guidance. Another issue of GPR surveys on glaciers that this

methodology helped to solve is the spatial resolution. The spatial coverage of GPR surveys is limited by survey speed, time and access (e.g. crevasses), leading to discrete, limited sampling of the glacier bed. It is, therefore, possible that the maximum ice thickness remains unknown due to limited survey coverage. Spatial resolution and speed of investigation have always been a compromise. With the use of constrained GlaTE model, the GPR analyst can provide a better ice-thickness estimation in those zone not surveyed by GPR, without having to rely on pure interpolation.

The integration of GPR and models seems the most viable option to provide a more reliable estimate of ice thickness than one method alone, especially in the absence of costly boreholes intercepting the bedrock at depth. This is a great achievement, because those models are open-source and require low effort to use, and their reliability and comparability with GPR data has been observed in this and previous research (Farinotti et al., 2017). They also can complement the design of a GPR survey to select the best antenna frequency, based on the expected ice depth, alongside forward modeling to produce synthetic data (MacGregor et al., 2021). Other geophysical surveys, such as Electrical or Seismic tomographies, could also be employed, but to reach more than 100 m of ice thickness, as needed in this glacier, one would need to set up very long profiles (>500m) and use powerful seismic or electrical sources: they are not as logistically convenient as the GPR.

However, many drawbacks have to be considered. First, the difficulties in interpreting the GPR data, which represent the most significant source of possible errors and subjectivity; then, inaccuracies in the estimates provided by the different models, which are a simplification of the real system, and rely on estimates of many parameters. However, the most delicate aspect which may limit this methodology is the balance between GPR and models. In fact, there is a concrete possibility of leaking the models into the observation, and in this sense, the human error element is key. In our opinion, the key to minimizing this potential error is to perform simulation on multiple models, display the GPR sections with multiple color scales and in both 2D and 3D environments, and acquire local knowledge about the studied glacier. Another source of error is the glacier perimeter, which is an important input of the models, because it was retrieved with a manual observation of the aerial orthophoto (Santin et al., 2023). Moreover, the fact that the DEM and the GPR surveys were carried out at different years required a time interpolation of the ice thickness, to take into account the progressive melting of ice, which introduced another deviation from the real value of ice thickness. The combination of multiple models and methods was key to minimizing the errors; however, the uncertainty remains a main factor in this kind of analysis and it is also difficult to estimate accurately (Aguayo et al., 2024; Shahateet et al., 2025). We observed a standard deviation of about 100 million m^3 of ice, which corresponds to an average ice thickness of about + - 13 meters, by comparing the three unconstrained models; we observed instead a standard deviation of about 75 million m^3 by comparing the unconstrained GlaTE model with varied glaciological parameters (sensitivity analysis). These values represent a reasonable estimate of the potential standard deviation in the ice thickness, but they are still biased by the choice of models used and the choice of the parameters to be varied in the sensitivity analysis. Moreover, the definition of standard deviation itself is probably not completely holding in this case, since it would need a Gaussian error distribution for the ice thicknesses estimated by the various models, which is probably not true. Interestingly, the standard deviation of ice volume calculated during the sensitivity analysis of the constrained GlaTE model is particularly low (about 5 million m^3), meaning that the constrained model is quite robust to variations in the input glaciological parameters and tries to adhere to the input GPR data, even if the given GPR data were quite sparse and they were assigned an uncertainty of 30 % in the GlaTE

input parameters. It is difficult to say if this very low standard deviation is indicative of real reliability of the GlaTE constrained model; nevertheless, 450 million m^3 of ice, distributed as in Figure 6, represents the best estimate of the Rutor glacier thickness we could obtain with this methodology.

A final and obvious limitation of the study is the absence of any borehole to confirm either the GPR and the model estimated thicknesses. Future research may consider to analyze glaciers where such borehole data is available. Nevertheless, in some decades, due to the ongoing glacier melting, we might directly see the current glacier bedrock in most parts of the glacier. These observations, together with the analysis of DEMs at different years, now possible due to the widespread satellite observations, will provide accurate geodetic mass balance information and surface topography that will allow to deepen the knowledge about ice flux behaviour in a non-equilibrium state and better calibrate the ice thickness models.

4.4 Future applications and perspectives

For different reasons, both the GPR and ice-thickness models have non-negligible accuracy limitations in reconstructing glacier geometry. The GPR suffers from scattering in temperate glaciers, while models alone have a high uncertainty based on which parameters we choose as input. The presentation of this methodology highlighted the importance, for future works, to combine the two worlds. For GPR practitioners, the use of models can help in designing the survey and selecting the proper instrumentation (e.g. antenna frequency) based on the estimated geometry of the glacier. Models can also provide a picture of the glacier in those zones unaccessible to GPR for logistics limitations or time constraints. For modelers, including GPR surveys in their workflow can improve their estimations, especially for those glaciers with complex and difficult-to-model geometries. In this sense, performing the little laborious work presented in this study, if performed on a bunch of relevant glaciers with GPR data available, could help calibrate regional models more accurately, or at least be more conscious of the potential uncertainties of the models. The supplementary materials can be used to reproduce the same workflow on other glaciers.

Future integration of GPR data in glacier models could include not only ice thickness, but other features of the glacier which are detected by GPR and are very difficult to predict with models, such as the distribution of cavities and the distinction between cold and warm ice zones inside a glacier. The latter, according to Reinardy et al. (2019) and Comiti et al. (2019), plays an important role in regulating the sediment transport at the glacier base, and can be retrieved from the distribution of reflections (due to englacial water) in the GPR sections. This could enhance the link between glacier geometry and hydrological output in a glacier model. The clutter itself in the radargram can be used to infer glacier features (Scanlan et al., 2020).

From a local perspective, a more robust reconstruction of the Rutor glacier compared to previous estimates will be helpful for ongoing studies on the water mass balance and sediment transport of the Rutor basin. Since the Rutor basin hosts many proglacial lakes, the map reveals the possible position of future lakes, in place of the overdeepenings of the bedrock topography (Figure 6). Their location is consistent with the estimates of a previous work (Viani et al., 2020). The shrinking of Rutor Glacier is speculated to occur mostly in the following decades, given its volume of about 450 million m^3 and its loss of 100 million m^3 from just 2008 to 2021. After a few decades, little ice is expected to be still stored in the Rutor Glacier.

5 Conclusions

Investigating glacier substructures with GPR may be challenging in temperate glaciers, where the widespread water content and debris cause signal scattering, making it difficult to distinguish the ice-bedrock interface. The Rutor Glacier had already been surveyed with GPR in the past but, due to these interpretation difficulties, was estimated to have a very small ice thickness, of about 17.5 m on average. This estimation proved to be wrong after observing that, in the 2010-2020 decade, the Rutor Glacier lost more than 20 vertical meters in 1/4 of its area, while reducing its area only by a fraction.

The analysis of two new GPR datasets from 2012 (helicopter-based) and 2022 (ground-based) confirmed the difficulty in reliably detecting the ice-bedrock interface. Therefore, the open-source GlabTop2, GlaTE, and OGGM models were tested, to understand how they could support the interpretation of difficult datasets acquired on temperate glaciers. First, those models were run with only the glacier surface topography as input. Then, their estimated thickness was overlapped with the GPR sections, providing substantial help in manually selecting the ice-bedrock interface. In particular, this methodology avoided misinterpreting englacial water-rich areas as the ice-bedrock interface. Finally, a second run of GlaTE produced an ice-thickness model of the Rutor Glacier constrained by GPR data.

Analyzing the ice-thickness variations among models and by varying the glaciological parameters of the GlaTE model, we recognized that the uncertainty in both GPR and models is a major factor and it is seriously difficult to measure a true value of ice thickness in a temperate glacier.

A prior run of two or three ice-thickness models, such as the ones tested in this study, is advised before carrying out a GPR survey on a glacier. The ice-thickness models, in combination with the GPR, are the most effort-effective way to represent, with a certain degree of uncertainty, a glacier bedrock geometry. This is in line with the philosophy behind the GlaTE model, built to constrain a topographical-data-based algorithm with "ground-proof" GPR data. An effort was made to provide supplementary materials which can be used to reproduce the same workflow on other glaciers. Local studies can benefit from more accurate glacier geometry estimations, as well as regional studies, which can be calibrated more effectively.

Code and data availability. All the data, codes and detailed reproducible workflow is available the Supplementary materials. We organized the Supplementary materials in 9 folders, each for each step of our workflow, each with a readme.txt file to describe the folder's contents, similar to a little methodological section. We invite the reader to download them and explore the proposed methodology on other glaciers.
The 2012 GPR dataset is available on a Zenodo repository at: https://doi.org/10.5281/zenodo.8027417
The 2021 DEM used for the GlaTE and GlabTop2 model, together with the ortophoto used to draw the glacier margin, is available on a Zenodo repository at: https://doi.org/10.5281/zenodo.7713299
Links at the main codes websites:
OGGM: https://oggm.org/
GlaTE: https://gitlab.com/hmaurer/glate
GlabTop2: https://glabtop2-py.readthedocs.io/en/latest/index.html

Author contributions. Conceptualization: A.V.; Data Curation: A.V.; Formal Analysis: A.V.; Funding Acquisition: A.G. and D.F.; Investigation: D.F.; Methodology: A.V., A.G. and D.F.; Project Administration: A.G.; Resources: A.G. and D.F.; Software: A.V; Supervision: A.G.; Validation: A.V.; Visualization: A.V; Writing: A.V..

Competing interests. The authors declare no competing interests are present.

Acknowledgements. Thanks to Umberto Morra di Cella and the regional environmental protection agency of Aosta Valley, Italy (ARPA Val d'Aosta) for the 2012 dataset. Thanks to Fabio Villa for his help in understanding the Rutor Glacier GPR and topography datasets. Thanks to Maurizio Ercoli, Emanuele Forte, Michele Freppaz and Chiara Colombero for their precious suggestions on the manuscript. Thanks to Myrta Maria Macelloni, Isabella Pisoni, Elisabetta Corte, and Alberto Cina for their help with the topographical data and for the 2021 Digital Elevation Model. Thanks to "CC-Glacier lab" of the MIUR project "Department of excellence" at the Politecnico di Torino—DIATI for funding part of this research. Thanks to Hansruedi Maurer and Melchior Grab for their help about the GlaTE model. Thanks to Emanuel Huber for his support about the RGPR open source software. Thanks to LeldeBry, mainainer of GlabTop2 Github repository, for his help with the model.

References

Aguayo, R., Maussion, F., Schuster, L., Schaefer, M., Caro, A., Schmitt, P., Mackay, J., Ultee, L., Leon-Muñoz, J., and Aguayo, M.: Unravelling the sources of uncertainty in glacier runoff projections in the Patagonian Andes (40–56° S), The Cryosphere, 18, 5383–5406, https://doi.org/10.5194/tc-18-5383-2024, 2024.

Ayachit, U.: The ParaView guide: updated for ParaView version 4.3, Kitware Inc, Clifton Park, NY, full color version edn., ISBN 978-1-930934-30-6, 2015.

Bohleber, P., Sold, L., Hardy, D. R., Schwikowski, M., Klenk, P., Fischer, A., Sirguey, P., Cullen, N. J., Potocki, M., Hoffmann, H., and Mayewski, P.: Ground-penetrating radar reveals ice thickness and undisturbed englacial layers at Kilimanjaro's Northern Ice Field, The Cryosphere, 11, 469–482, https://doi.org/10.5194/tc-11-469-2017, 2017.

Church, G. J., Bauder, A., Grab, M., Hellmann, S., and Maurer, H.: High-resolution helicopter-borne ground penetrating radar survey to determine glacier base topography and the outlook of a proglacial lake, in: 2018 17th International Conference on Ground Penetrating Radar (GPR), pp. 1–4, IEEE, Rapperswil, Switzerland, ISBN 978-1-5386-5777-5, https://doi.org/10.1109/ICGPR.2018.8441598, 2018.

Clarke, G. K. C., Anslow, F. S., Jarosch, A. H., Radić, V., Menounos, B., Bolch, T., and Berthier, E.: Ice Volume and Subglacial Topography for Western Canadian Glaciers from Mass Balance Fields, Thinning Rates, and a Bed Stress Model, Journal of Climate, 26, 4282–4303, https://doi.org/10.1175/JCLI-D-12-00513.1, 2013.

Colombero, C., Comina, C., De Toma, E., Franco, D., and Godio, A.: Ice Thickness Estimation from Geophysical Investigations on the Terminal Lobes of Belvedere Glacier (NW Italian Alps), Remote Sensing, 11, 805, https://doi.org/10.3390/rs11070805, 2019.

Colucci, R. R., Forte, E., Boccali, C., Dossi, M., Lanza, L., Pipan, M., and Guglielmin, M.: Evaluation of Internal Structure, Volume and Mass of Glacial Bodies by Integrated LiDAR and Ground Penetrating Radar Surveys: The Case Study of Canin Eastern Glacieret (Julian Alps, Italy), Surveys in Geophysics, 36, 231–252, https://doi.org/10.1007/s10712-014-9311-1, 2015.

Comiti, F., Mao, L., Penna, D., Dell'Agnese, A., Engel, M., Rathburn, S., and Cavalli, M.: Glacier melt runoff controls bedload transport in Alpine catchments, Earth and Planetary Science Letters, 520, 77–86, https://doi.org/10.1016/j.epsl.2019.05.031, 2019.

Cook, S. J., Swift, D. A., Kirkbride, M. P., Knight, P. G., and Waller, R. I.: The empirical basis for modelling glacial erosion rates, Nature Communications, 11, 759, https://doi.org/10.1038/s41467-020-14583-8, 2020.

Corte, E., Ajmar, A., Camporeale, C., Cina, A., Coviello, V., Giulio Tonolo, F., Godio, A., Macelloni, M. M., Tamea, S., and Vergnano, A.: Multitemporal characterization of a proglacial system: a multidisciplinary approach, Earth System Science Data, 16, 3283–3306, https://doi.org/10.5194/essd-16-3283-2024, 2024.

Crameri, F.: Scientific colour maps, https://doi.org/10.5281/ZENODO.1243862, language: en, 2021.

Cuffey, K. M. and Paterson, W. S. B.: The physics of glaciers, Elsevier, San Diego, fourth edition edn., ISBN 978-0-12-369461-4 978-0-08-091912-6, 2010.

Farinotti, D., Huss, M., Bauder, A., Funk, M., and Truffer, M.: A method to estimate the ice volume and ice-thickness distribution of alpine glaciers, Journal of Glaciology, 55, 422–430, https://doi.org/10.3189/002214309788816759, 2009.

Farinotti, D., Brinkerhoff, D. J., Clarke, G. K. C., Fürst, J. J., Frey, H., Gantayat, P., Gillet-Chaulet, F., Girard, C., Huss, M., Leclercq, P. W., Linsbauer, A., Machguth, H., Martin, C., Maussion, F., Morlighem, M., Mosbeux, C., Pandit, A., Portmann, A., Rabatel, A., Ramsankaran, R., Reerink, T. J., Sanchez, O., Stentoft, P. A., Singh Kumari, S., van Pelt, W. J. J., Anderson, B., Benham, T., Binder, D., Dowdeswell, J. A., Fischer, A., Helfricht, K., Kutuzov, S., Lavrentiev, I., McNabb, R., Gudmundsson, G. H., Li, H., and Andreassen,

L. M.: How accurate are estimates of glacier ice thickness? Results from ITMIX, the Ice Thickness Models Intercomparison eXperiment, The Cryosphere, 11, 949–970, https://doi.org/10.5194/tc-11-949-2017, 2017.

Farinotti, D., Huss, M., Fürst, J. J., Landmann, J., Machguth, H., Maussion, F., and Pandit, A.: A consensus estimate for the ice thickness distribution of all glaciers on Earth, Nature Geoscience, 12, 168–173, https://doi.org/10.1038/s41561-019-0300-3, 2019.

Forte, E., Pipan, M., Francese, R., and Godio, A.: An overview of GPR investigation in the Italian Alps, First Break, 33, https://doi.org/10.3997/1365-2397.33.8.82011, 2015.

Forte, E., Santin, I., Ponti, S., Colucci, R. R., Gutgesell, P., and Guglielmin, M.: New insights in glaciers characterization by differential diagnosis integrating GPR and remote sensing techniques: A case study for the Eastern Gran Zebrù glacier (Central Alps), Remote Sensing of Environment, 267, 112 715, https://doi.org/10.1016/j.rse.2021.112715, 2021.

Frey, H., Machguth, H., Huss, M., Huggel, C., Bajracharya, S., Bolch, T., Kulkarni, A., Linsbauer, A., Salzmann, N., and Stoffel, M.: Estimating the volume of glaciers in the Himalayan–Karakoram region using different methods, The Cryosphere, 8, 2313–2333, https://doi.org/10.5194/tc-8-2313-2014, 2014.

Gizzi, M., Mondani, M., Taddia, G., Suozzi, E., and Lo Russo, S.: Aosta Valley Mountain Springs: A Preliminary Analysis for Understanding Variations in Water Resource Availability under Climate Change, Water, 14, 1004, https://doi.org/10.3390/w14071004, 2022.

Glen, J. W. and Paren, J. G.: The Electrical Properties of Snow and Ice, Journal of Glaciology, 15, 15–38, https://doi.org/10.3189/S0022143000034249, 1975.

Grab, M., Mattea, E., Bauder, A., Huss, M., Rabenstein, L., Hodel, E., Linsbauer, A., Langhammer, L., Schmid, L., Church, G., Hellmann, S., Délèze, K., Schaer, P., Lathion, P., Farinotti, D., and Maurer, H.: Ice thickness distribution of all Swiss glaciers based on extended ground-penetrating radar data and glaciological modeling, Journal of Glaciology, 67, 1074–1092, https://doi.org/10.1017/jog.2021.55, 2021.

Haeberli, W. and Hoelzle, M.: Application of inventory data for estimating characteristics of and regional climate-change effects on mountain glaciers: a pilot study with the European Alps, Annals of Glaciology, 21, 206–212, https://doi.org/10.3189/S0260305500015834, 1995.

Haeberli, W., Oerlemans, J., and Zemp, M.: The Future of Alpine Glaciers and Beyond, in: Oxford Research Encyclopedia of Climate Science, Oxford University Press, ISBN 978-0-19-022862-0, https://doi.org/10.1093/acrefore/9780190228620.013.769, 2019.

Huber, E. and Hans, G.: RGPR — An open-source package to process and visualize GPR data, in: 2018 17th International Conference on Ground Penetrating Radar (GPR), pp. 1–4, IEEE, Rapperswil, ISBN 978-1-5386-5777-5, https://doi.org/10.1109/ICGPR.2018.8441658, 2018.

Hugonnet, R., McNabb, R., Berthier, E., Menounos, B., Nuth, C., Girod, L., Farinotti, D., Huss, M., Dussaillant, I., Brun, F., and Kääb, A.: Accelerated global glacier mass loss in the early twenty-first century, Nature, 592, 726–731, https://doi.org/10.1038/s41586-021-03436-z, 2021.

Jol, H. M.: Ground penetrating radar theory and applications, Elsevier Science, Amsterdam, Netherlands, 1st edn., ISBN 978-0-08-095184-3, oCLC: 1078275154, 2009.

Karušs, J., Lamsters, K., Ješkins, J., Sobota, I., and Džeriņš, P.: UAV and GPR Data Integration in Glacier Geometry Reconstruction: A Case Study from Irenebreen, Svalbard, Remote Sensing, 14, 456, https://doi.org/10.3390/rs14030456, 2022.

Lange, S.: WFDE5 over land merged with ERA5 over the ocean (W5E5), https://doi.org/10.5880/PIK.2019.023, 2019.

Langhammer, L., Grab, M., Bauder, A., and Maurer, H.: Glacier thickness estimations of alpine glaciers using data and modeling constraints, The Cryosphere, 13, 2189–2202, https://doi.org/10.5194/tc-13-2189-2019, 2019a.

Langhammer, L., Rabenstein, L., Schmid, L., Bauder, A., Grab, M., Schaer, P., and Maurer, H.: Glacier bed surveying with helicopter-borne dual-polarization ground-penetrating radar, Journal of Glaciology, 65, 123–135, https://doi.org/10.1017/jog.2018.99, 2019b.

Langley, K., Lacroix, P., Hamran, S.-E., and Brandt, O.: Sources of backscatter at 5.3 GHz from a superimposed ice and firn area revealed by multi-frequency GPR and cores, Journal of Glaciology, 55, 373–383, https://doi.org/10.3189/002214309788608660, 2009.

Linsbauer, A., Paul, F., and Haeberli, W.: Modeling glacier thickness distribution and bed topography over entire mountain ranges with GlabTop: Application of a fast and robust approach: REGIONAL-SCALE MODELING OF GLACIER BEDS, Journal of Geophysical Research: Earth Surface, 117, https://doi.org/10.1029/2011JF002313, 2012.

Macelloni, M. M., Corte, E., Ajmar, A., Cina, A., Giulio Tonolo, F., Maschio, P. F., and Pisoni, I. N.: Multi-platform, Multi-scale and Multi-temporal 4D Glacier Monitoring. The Rutor Glacier Case Study, in: Geomatics for Green and Digital Transition, edited by Borgogno-Mondino, E. and Zamperlin, P., vol. 1651, pp. 392–404, Springer International Publishing, Cham, ISBN 978-3-031-17438-4 978-3-031-17439-1, https://doi.org/10.1007/978-3-031-17439-1_29, series Title: Communications in Computer and Information Science, 2022.

MacGregor, J. A., Studinger, M., Arnold, E., Leuschen, C. J., Rodríguez-Morales, F., and Paden, J. D.: Brief communication: An empirical relation between center frequency and measured thickness for radar sounding of temperate glaciers, The Cryosphere, 15, 2569–2574, https://doi.org/10.5194/tc-15-2569-2021, 2021.

Maurer, H.: GlaTE - Glacier thickness modeling algorithm, https://gitlab.com/hmaurer/glate, 2022.

Maussion, F.: OGGM - Open Global Glacier Model, https://github.com/OGGM/oggm, 2024.

Maussion, F., Butenko, A., Champollion, N., Dusch, M., Eis, J., Fourteau, K., Gregor, P., Jarosch, A. H., Landmann, J., Oesterle, F., Recinos, B., Rothenpieler, T., Vlug, A., Wild, C. T., and Marzeion, B.: The Open Global Glacier Model (OGGM) v1.1, Geoscientific Model Development, 12, 909–931, https://doi.org/10.5194/gmd-12-909-2019, 2019.

Millan, R., Mouginot, J., Rabatel, A., and Morlighem, M.: Ice velocity and thickness of the world's glaciers, Nature Geoscience, 15, 124–129, https://doi.org/10.1038/s41561-021-00885-z, 2022.

Milner, A. M., Khamis, K., Battin, T. J., Brittain, J. E., Barrand, N. E., Füreder, L., Cauvy-Fraunié, S., Gíslason, G. M., Jacobsen, D., Hannah, D. M., Hodson, A. J., Hood, E., Lencioni, V., Ólafsson, J. S., Robinson, C. T., Tranter, M., and Brown, L. E.: Glacier shrinkage driving global changes in downstream systems, Proceedings of the National Academy of Sciences, 114, 9770–9778, https://doi.org/10.1073/pnas.1619807114, 2017.

Morra di Cella, U.: Helicopter-based GPR survey of Rutor glacier and nearby glaciers, Aosta Valley, Italy, in May 2012, https://doi.org/10.5281/zenodo.8027417, 2024.

QGIS Development Team: QGIS Geographic Information System, http://qgis.osgeo.org, 2021.

Reinardy, B. T. I., Booth, A. D., Hughes, A. L. C., Boston, C. M., Åkesson, H., Bakke, J., Nesje, A., Giesen, R. H., and Pearce, D. M.: Pervasive cold ice within a temperate glacier – implications for glacier thermal regimes, sediment transport and foreland geomorphology, The Cryosphere, 13, 827–843, https://doi.org/10.5194/tc-13-827-2019, 2019.

RGI Consortium, R. G. I.: Randolph Glacier Inventory 6.0, https://doi.org/10.7265/N5-RGI-60, 2017.

Rutishauser, A., Maurer, H., and Bauder, A.: Helicopter-borne ground-penetrating radar investigations on temperate alpine glaciers: A comparison of different systems and their abilities for bedrock mapping, Geophysics, 81, WA119–WA129, https://doi.org/10.1190/geo2015-0144.1, 2016.

Sandmeier, K.: REFLEXW Version 7.0-program for the Processing of Seismic, Acoustic or Electromagnetic Reflection, Refraction and Transmission Data, User's Manual, 578, https://www.sandmeier-geo.de/guides-and-videos.html, 2012.

Santin, I., Forte, E., Nicora, M., Ponti, S., and Guglielmin, M.: Where does a glacier end? Integrated geophysical, geomorphological and photogrammetric measurements to image geometry and ice facies distribution, Catena, 225, 107 016, https://doi.org/10.1016/j.catena.2023.107016, 2023.

Scanlan, K. M., Rutishauser, A., Young, D. A., and Blankenship, D. D.: Interferometric discrimination of cross-track bed clutter in ice-penetrating radar sounding data, Annals of Glaciology, 61, 68–73, https://doi.org/10.1017/aog.2020.20, 2020.

Schwanghart, W. and Scherler, D.: Short Communication: TopoToolbox 2 – MATLAB-based software for topographic analysis and modeling in Earth surface sciences, Earth Surface Dynamics, 2, 1–7, https://doi.org/10.5194/esurf-2-1-2014, 2014.

Shahateet, K., J. Fürst, J., Navarro, F., Seehaus, T., Farinotti, D., and Braun, M.: A reconstruction of the ice thickness of the Antarctic Peninsula Ice Sheet north of 70° S, The Cryosphere, 19, 1577–1597, https://doi.org/10.5194/tc-19-1577-2025, 2025.

Suter, S., Laternser, M., Haeberli, W., Frauenfelder, R., and Hoelzle, M.: Cold firn and ice of high-altitude glaciers in the Alps: measurements and distribution modelling, Journal of Glaciology, 47, 85–96, https://doi.org/10.3189/172756501781832566, 2001.

Terink, W.: GlabTop2-py, https://github.com/WilcoTerink/GlabTop2-py;https://glabtop2-py.readthedocs.io/en/latest/index.html, 2018.

Urbini, S., Bianchi-Fasani, G., Mazzanti, P., Rocca, A., Vittuari, L., Zanutta, A., Girelli, V. A., Serafini, M., Zirizzotti, A., and Frezzotti, M.: Multi-Temporal Investigation of the Boulder Clay Glacier and Northern Foothills (Victoria Land, Antarctica) by Integrated Surveying Techniques, Remote Sensing, 11, 1501, https://doi.org/10.3390/rs11121501, 2019.

Val d'Aosta Region: Servizi Cartografici SCT - GeoDownload, https://mappe.regione.vda.it/pub/geonavitg/geodownload.asp?carta=DTM99, 2008.

Vergnano, A., Oggeri, C., and Godio, A.: Geophysical–geotechnical methodology for assessing the spatial distribution of glacio-lacustrine sediments: The case history of Lake Seracchi, Earth Surface Processes and Landforms, p. esp.5555, https://doi.org/10.1002/esp.5555, 2023.

Viani, C., Machguth, H., Huggel, C., Perotti, L., and Giardino, M.: Detecting glacier-bed overdeepenings for glaciers in the Western Italian Alps using the GlabTop2 model: the test site of the Rutor Glacier, Aosta Valley, in: EGU General Assembly Conference Abstracts, pp. EPSC2016–13 607, 2016.

Viani, C., Machguth, H., Huggel, C., Godio, A., Franco, D., Perotti, L., and Giardino, M.: Potential future lakes from continued glacier shrinkage in the Aosta Valley Region (Western Alps, Italy), Geomorphology, 355, 107 068, https://doi.org/10.1016/j.geomorph.2020.107068, 2020.

Villa, F., De Amicis, M., and Maggi, V.: GIS analysis of Rutor Glacier (Aosta Valley, Italy) volume and terminus variations, Geografia Fisica e Dinamica Quaternaria, 30, 87–95, www.scopus.com, 2007.

Villa, F., Tamburini, A., Deamicis, M., Sironi, S., Maggi, V., and Rossi, G.: Volume decrease of Rutor Glacier (Western Italian Alps) since little ice age: A quantitative approach combining GPR, GPS and cartography, Geografia Fisica e Dinamica Quaternaria, 31, 63–70, www.scopus.com, 2008.

Weertman, J.: Mechanism for the Formation of Inner Moraines Found Near the Edge of Cold Ice Caps and Ice sheets, Journal of Glaciology, 3, 965–978, https://doi.org/10.3189/S0022143000017378, 1961.

Zekollari, H., Huss, M., Farinotti, D., and Lhermitte, S.: Ice-Dynamical Glacier Evolution Modeling—A Review, Reviews of Geophysics, 60, e2021RG000 754, https://doi.org/10.1029/2021RG000754, 2022.

Appendix A: Appendix - GPR Sections

This appendix is devoted to all the GPR sections analyzed in this work, to show the interested reader what the data looked like, which were the difficulties, and in which cases the three models' predictions were useful in avoiding clear misinterpretations. In any case, the interpretation subjectivity is high, and analyzing the openly available GPR dataset with specialistic software is advised. The first 5 figures represent the 5 GPR sections of the 2012 heli-based survey; the last figure is the merging of all (subsequent) sections of the 2022 ground-based survey. See Figure 6 for the location of the GPR sections.

Additional figures at the end of the appendix show: a 3D visualization of models and GPR in Paraview (Figure A7); a map of the bedrock and surface topography as in the constrained GlaTE model, visualized in contour lines (Figure A8); a comparison with literature ice-thickness products (Figure A9).

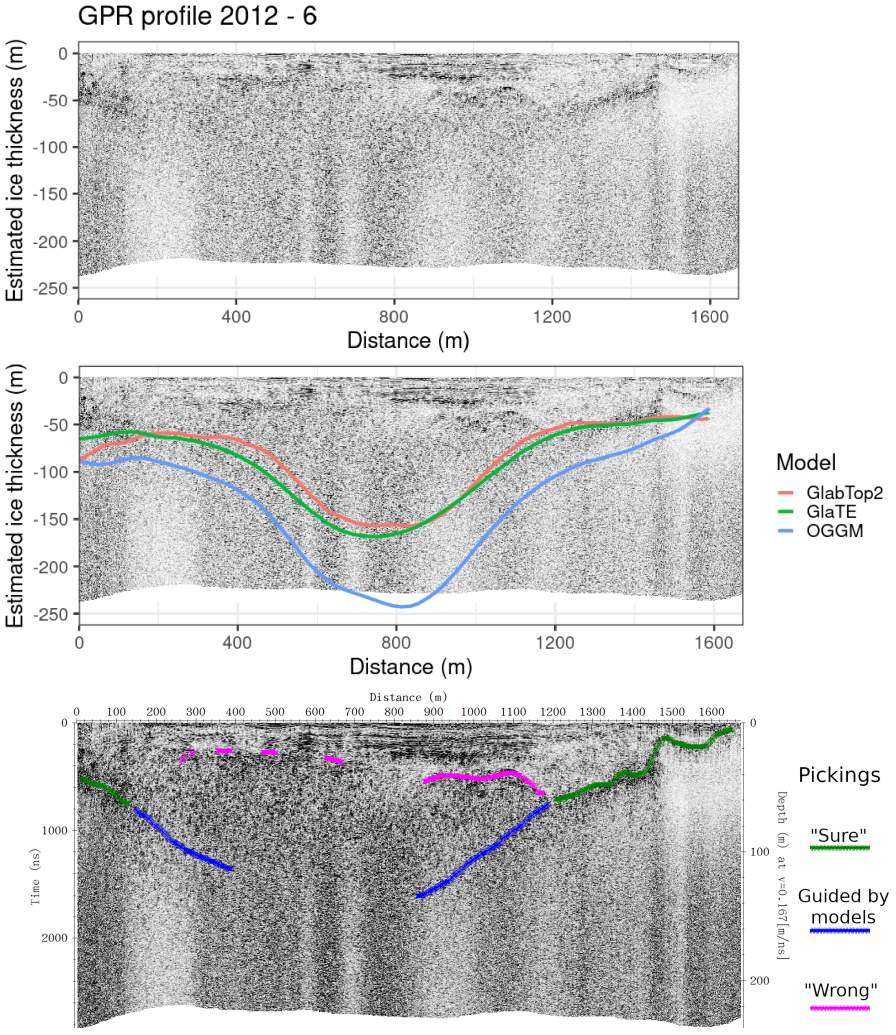

Figure A1. GPR section 2012 - 6. This section is situated at the top of the glacier, and in its central part (500-1000 m of Distance coordinate) the three models estimate an overdeepening of over 150 m. The GPR reflections are reasonably clear until 50-70 m of depth. In the right part of the picture, the models follow closely the GPR reflections; however, they are quite imprecise just near the margin, where they do not draw correctly the bedrock shape where the ice is very thin. Based on the estimates of the models, the analyst did not trusted the sparse reflections at 25-30 m depth as an ice-bedrock interface but acknowledged that, in the right part, the deepening reflections continue to go deeper leftward until around the center of the image.

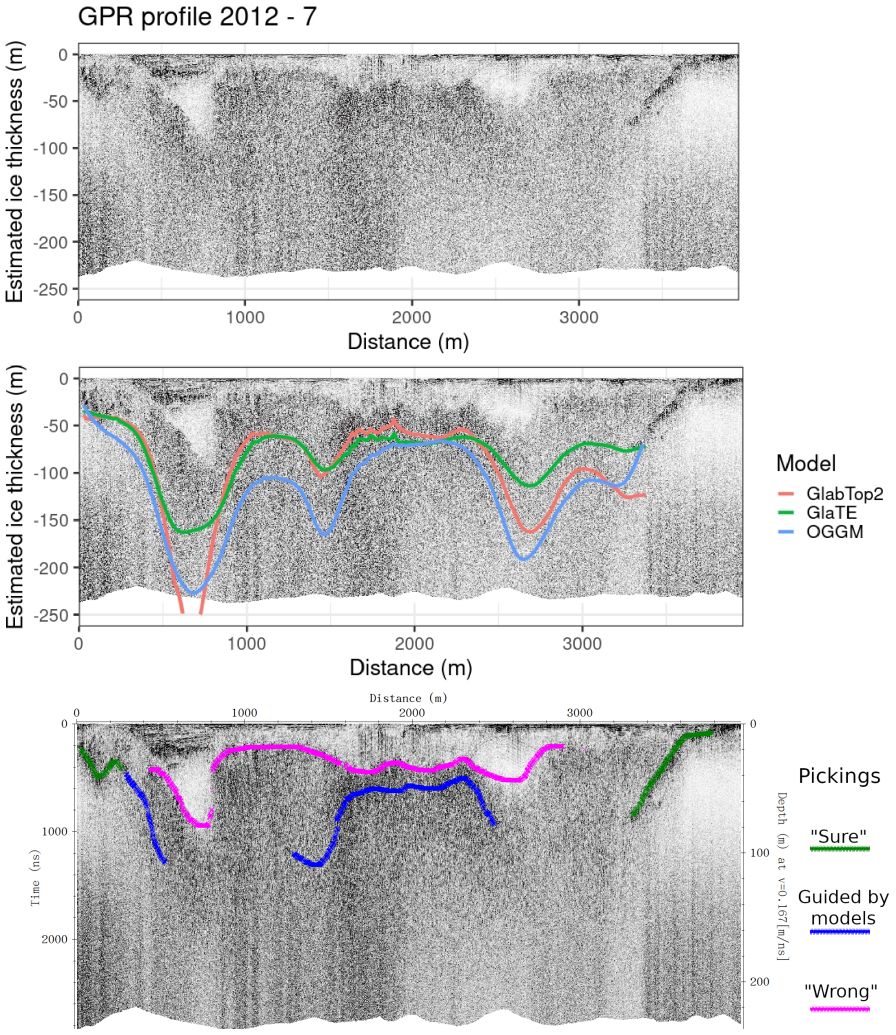

Figure A2. GPR section 2012 - 7. This section was already shown and discussed in Figure 5, but it is possible to add a consideration on the steep overdeepening "seen" by the GlabTop2 model. The creation of deep overdeepenings was recognized to be an artifact of such models, especially when using a too-fine input DEM [Maurer and Grab, personal communication]. Also, the other models estimate a high ice thickness at that point, but they seem more realistic. Unfortunately, the GPR was of little help in that region.

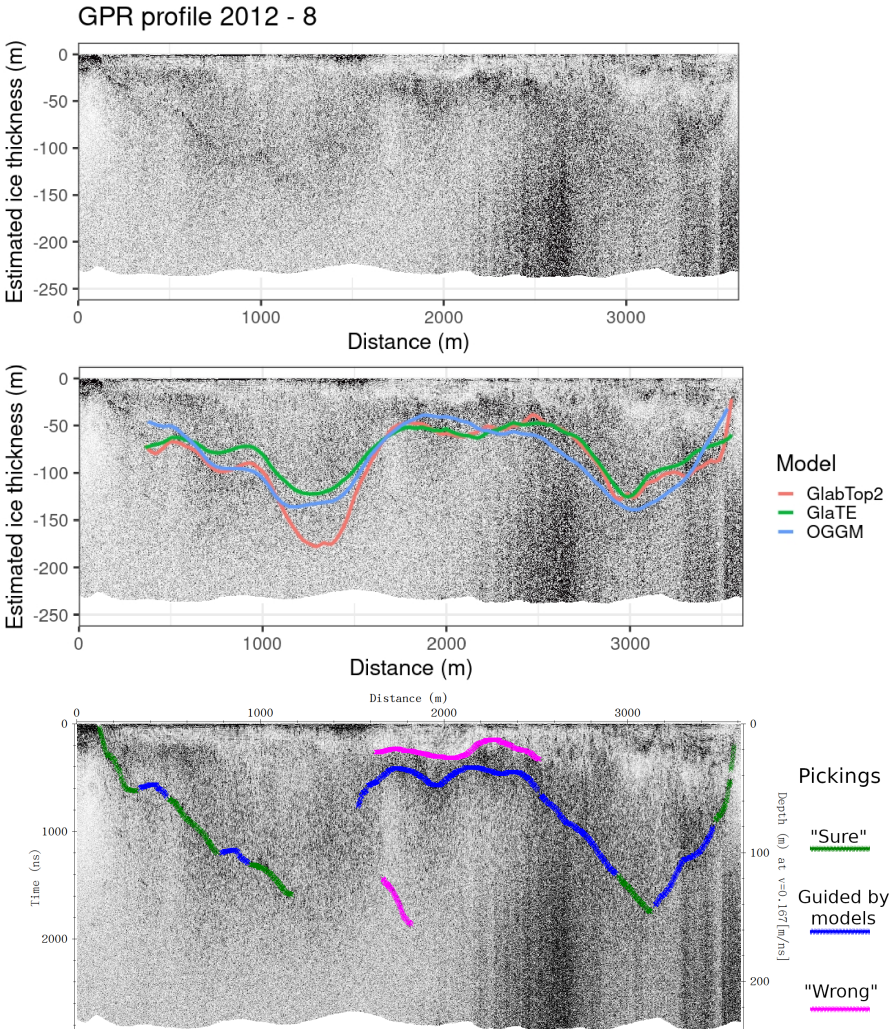

Figure A3. GPR section 2012 - 8. This GPR section was probably the most clear of the dataset. The ice-bedrock reflector can be followed in almost all the images to great depths, although the clarity is far from ideal. This section can be considered proof that the models are capable of doing reasonable estimates of the ice thickness in Rutor Glacier. In the left part of the image, which corresponds to the Eastern tongue, the models are not shown because they were cut with the 2021 margin. From 2012 to 2021, the glacier experienced a notable retreat. in the Eastern tongue.

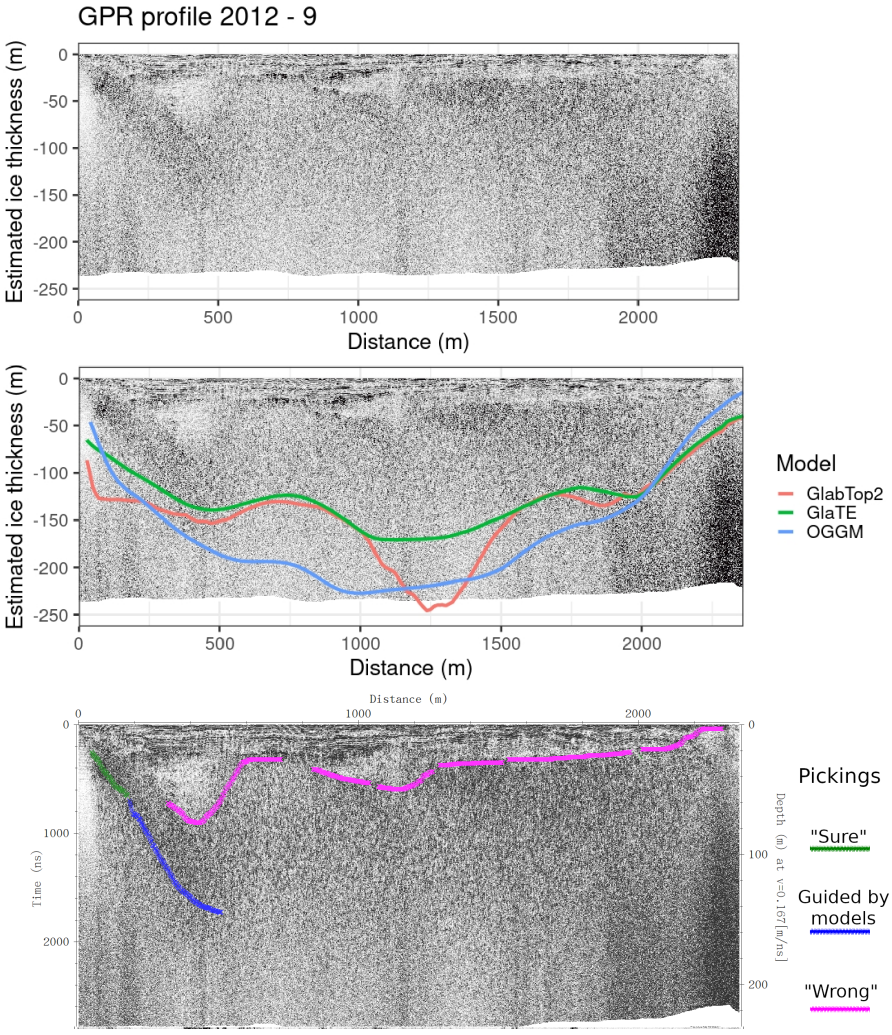

Figure A4. GPR section 2012 - 9. This GPR section was probably the least clear. Its path runs along the elongated overdeepening of the top of the glacier (Figure 6). In the left part of the picture, the reflections deepen very fast, and this is reproduced also by the models, but after that, it was impossible to retrieve any other reflections attributable to the ice-bedrock interface. The role of the models, in this case, was very important, to avoid thinking that the darker reflections seen in the center-right part of the image at 30-50 m depth are the bedrock interface, while probably it is due to the higher englacial water content, or debris (Forte et al., 2021).

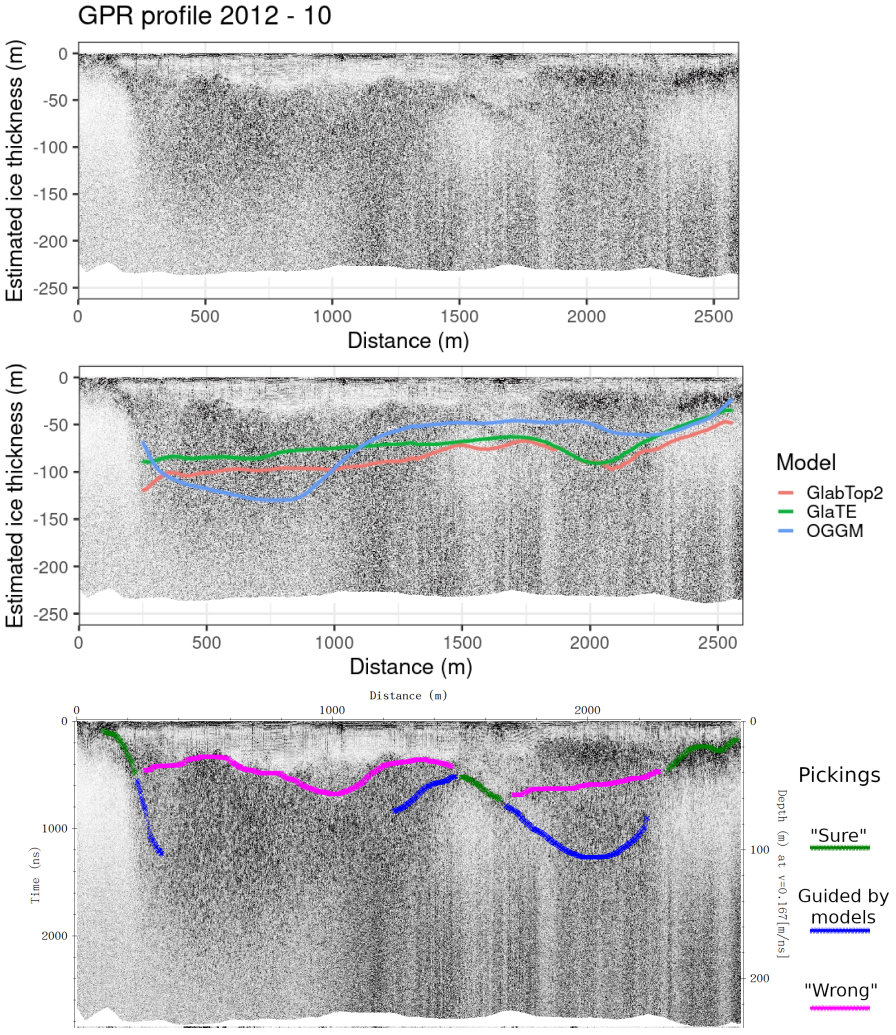

Figure A5. GPR section 2012 - 10. This GPR section was generally clear in the right part of the image and also showed consistency between GPR and models. All the profile has an interface around 30-40 m interpreted as englacial water or debris (Forte et al., 2021). The left part of the picture was more problematic, because the GPR, although not clear, seems to suggest a deeper bedrock interface than the models. Probably, this is due to a very problematic location of this survey line, possibly running along a very high-sloping bedrock (Figure 6). Such high-slope bedrock areas are known to disrupt GPR measurements and they could be common near the overdeepenings of Rutor Glacier since they are also evidenced in many locations in the proglacial zone (which was formerly occupied by ice during the glaciations).

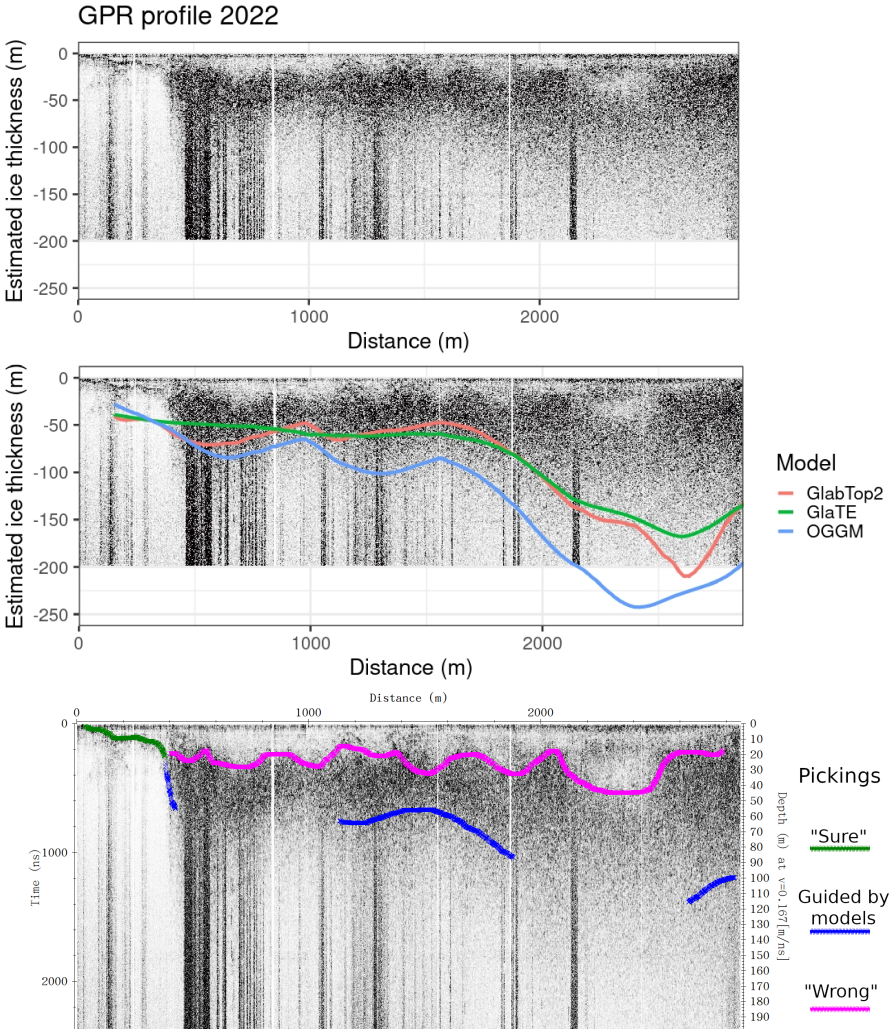

Figure A6. GPR section 2022. This GPR section was acquired with an antenna (40 MHz) different from that used for the previous sections shown. It also was ground-based and not helicopter-based. Notwithstanding the lower frequency and being ground-based, the GPR reflections were not particularly clearer, showing a physical limit of the technology in the presence of widespread englacial water or debris (Forte et al., 2021). The models did not perform well near the margin, as observed quite everywhere. However, probably they offer a reasonable estimate of the bedrock interface in all the left-central part of the image. The right part seems more problematic because the GPR signal is completely lost, however, its greater depth is supported by the GPR signal texture: compare e.g. the image at 100 m depth at Distance = 1000 m and = 2500 m. At distance = 2500 m, the image shows a granular texture similar to where there is ice and englacial water, while at Distance = 1000 m the texture is transparent. Similar considerations were used to interpret the GPR sections by Forte et al. (2021).

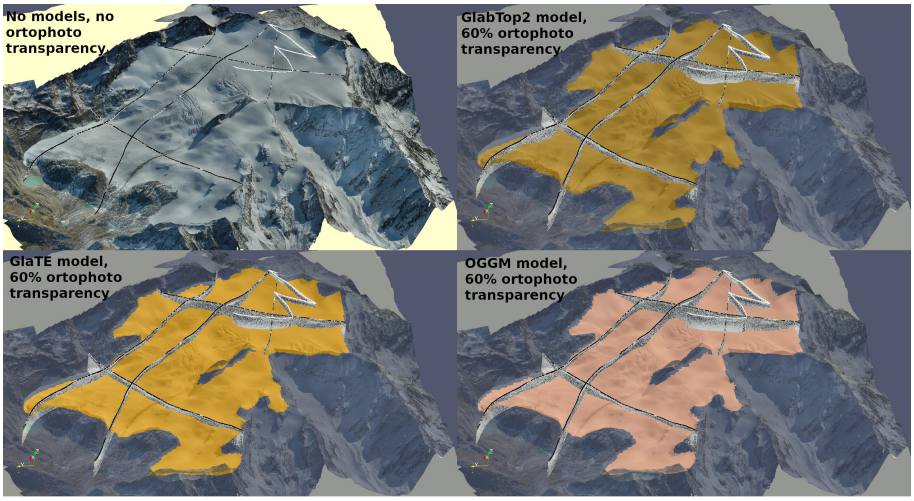

Figure A7. 3D visualization in Paraview of GPR profiles and bedrock as estimated by the three models. This 3D visualization, even if difficult to render in a 2D image, was helpful to see the GPR profiles at their intersections, where their bedrock interface must match.

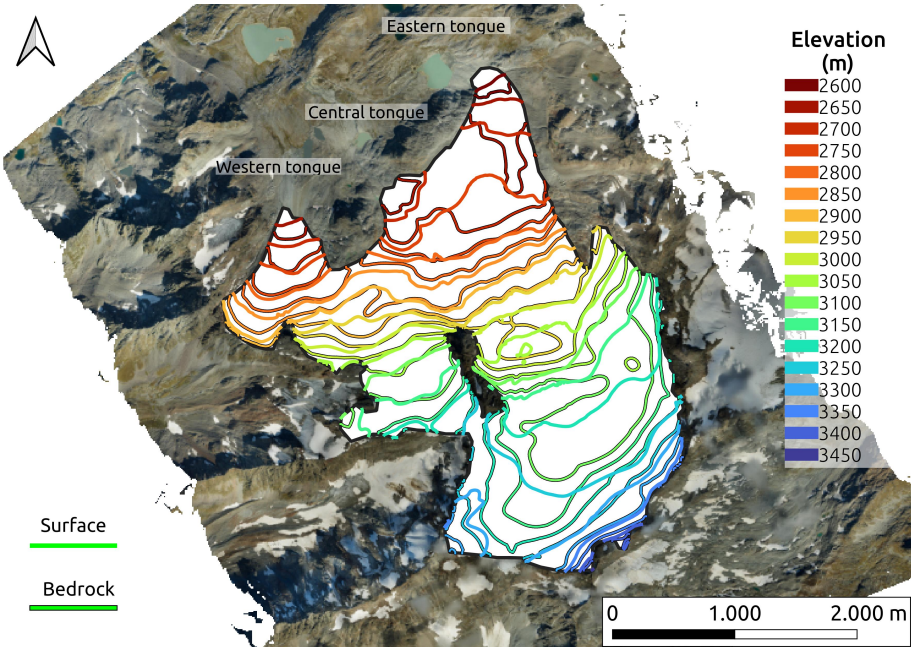

Figure A8. Bedrock and surface contour lines as in the constrained GlaTE model.

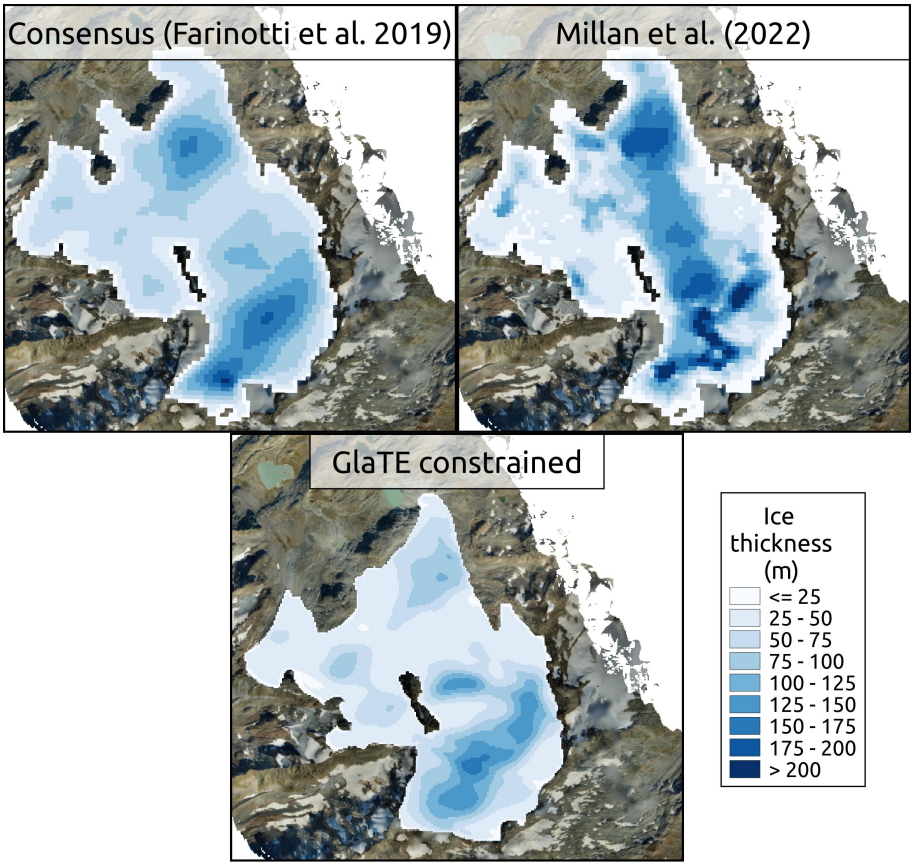

Figure A9. Comparison between the ice-thickness product of the constrained GlaTE model and two literature products: an ice-thickness map by Millan et al. (2022) and the consensus estimate (Farinotti et al., 2019).